# Single-cell Glycogenomics Deciphers Links Between Altered Transcriptional Regulation and Aberrant Glycosylation in Alzheimer's Disease

Yusuke Matsui*[1,2], Akira Togayachi[3], Kazuma Sakamoto[1,4], Kiyohiko Angata[3], Kenji Kadomatsu[1,4], Shoko Nishihara[3].

[1]Institute for Glyco-core Research (iGCORE), Nagoya University, Furo-cho, Chikusa-ku, Nagoya 464-8601, Japan

[2]Biomedical and Health Informatics Unit, Department of Integrated Health Science, Nagoya University Graduate School of Medicine, Daiko-minami, Higashi-ku, Nagoya, 461-8673, Japan

[3]Glycan and Life Systems Integration Center (GaLSIC), Soka University, 1-236 Tangi-machi, Hachioji, Tokyo 192-8577, Japan

[4]Department of Biochemistry, Nagoya University Graduate School of Medicine, Tsurumai-cho, Showa-ku, Nagoya, 466-8550, Japan

*Corresponding author

Lead Contact: matsui@met.nagoya-u.ac.jp

## Graphical Abstract

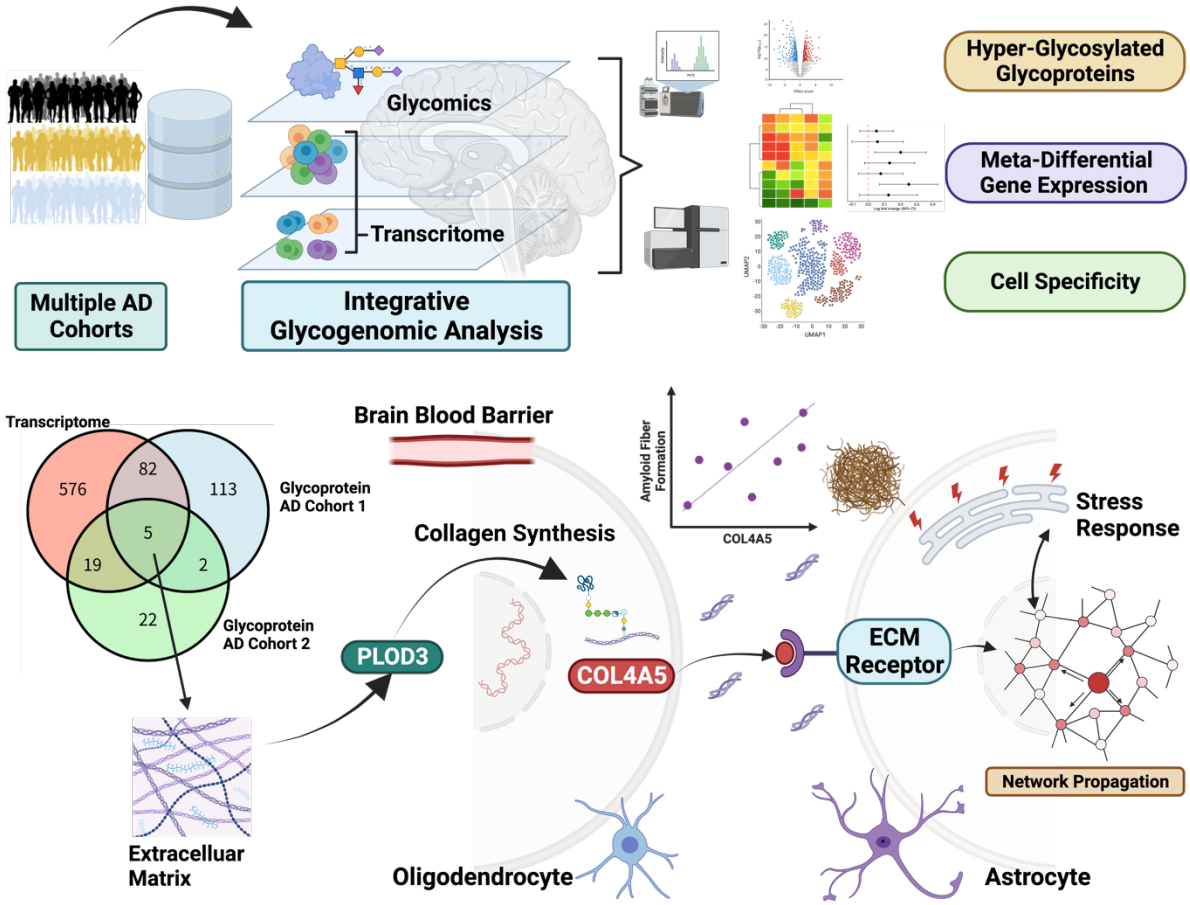

**Summary**

Glycosylation is increasingly recognized as a potential new therapeutic target in Alzheimer's disease. In recent years, evidence for Alzheimer's disease-specific glycoproteins has been established. However, the mechanisms of their dysregulation, including tissue and cell type specificity, are not fully understood. We aimed to explore upstream regulators of aberrant glycosylation by integrating multiple data sources and using a glycogenomics approach. We identified dysregulation by the glycosyltransferase PLOD3 in oligodendrocytes as an upstream regulator in cerebral vessels, and found that it is involved in COL4A5 synthesis, which is strongly correlated with amyloid fiber formation. Furthermore, COL4A5 was suggested to interact with astrocytes via ECM receptors as a ligand. This study suggests directions for new therapeutic strategies for Alzheimer's disease targeting glycosyltransferases.

35 **Introduction**

36 Alzheimer's disease (AD) is an age-related neurodegenerative disease[1,2]. It's primary
37 causes are neurogenic cell loss, accumulation of misfolded proteins, oxidative stress, and
38 inflammatory responses[3]. In previous studies, genomic, transcriptomic, epigenetic
39 mechanisms have been intensively examined[4]. However, our knowledge of post-translational
40 modifications that regulate cellular functions and interactions between cells remain still
41 lacking[5]. In particular, glycosylation is the most diverse and abundant post-translational
42 modification among protein modifications[6].

43 Glycosylation to proteins is a complex multi-step process involving approximately 200
44 different glycosyltransferases[6–8]. There are 16 major glycosylation pathways known, including
45 lipid glycosylation, N-glycosylation, O-glycosylation, C-mannosylation, lipid glycosylation,
46 and GPI-anchored synthesis. Recently, glycomics analysis of human AD postmortem brain[9,10],
47 serum[11–17] and cerebrospinal fluid[18–20] for N-glycosylation, the most abundant glycosylation
48 pathway, has revealed a dysregulated glycoproteins. Also, biological functions of abnormal
49 glycans in AD pathology have been reported in some cases, for example, it is known that
50 inhibition of BACE1 glycosylation reduces cleavage of β precursor protein (APP) [21–23]. However,
51 most of the biological functions of glycosylation in the pathogenesis of AD is poorly understood.

52 Glycan structures themselves are not independent of DNA template, and the
53 glycosylation depends on the combination of about 200 glycosyltransferases and about 500
54 related proteins[6–8] . Thus, their dysregulation could be an upstream regulatory factor that
55 triggers abnormal glycosylation processes[24]. Besides it is difficult to elucidate biological
56 glycosylation mechanisms at the single cell resolution by glycomics alone since current
57 technology is limited to probing by glycosylation-specific antibodies and glycan-binding
58 proteins (GBP, lectin, etc.) [6]. Therefore a glycogenomics approach that integrates genomics or
59 functional genomics and glycomics is critical for a comprehensive understanding for biological
60 glycosylation pathways[24,25].

We present upstream factors of aberrant glycosylation in AD. To this end, we performed an integrated analysis of bulk and single-cell/nucleus transcriptomic and glycomics data in human AD brain tissue. In particular, we show that the extracellular matrix (ECM) is a common signature in glycome and transcriptome, and that their expression signatures are enriched for cerebral vascular-related pathways. We identify Procollagen-Lysine,2-Oxoglutarate 5-Dioxygenase 3 (PLOD3) as an upstream glycosyltransferase common to these mechanisms, and through integrated analysis of multiple single-cell expression data. We show that PLOD3 is involved in the regulation of the collagen type IV alpha 5 chain (COL4A5). It is strongly correlated with amyloid fiber formation activity. Cell-cell interaction and signaling pathway analyses suggest that they are involved in the stress response via the ECM receptor on astrocytes.

**Hyperglycosylated proteins are primarily enriched in the extracellular matrix**

To examine the association between AD molecular pathogenesis and glycosylation, we accessed glycomics data consisting of two cohorts of postmortem brain tissue from AD patients [9,10] (**Figure 1A**). The first dataset consisted of eight neuropathologically confirmed AD cases and eight age-matched controls in dorsolateral prefrontal cortex tissue. Another dataset was a subset of the ROSMAP cohort[14]. Glycomics was performed on the postmortem brains of 10 patients with asymptomatic AD, 10 patients with symptomatic AD, and 10 normal brains in which none of the above were present.

In each cohort, 92 and 10 AD-specific hyperglycosylated proteins (**Supplementary Table S1**) were identified and pathway enrichment analysis was performed on them (**Figure 1A**). Among the pathways significantly enriched in the two cohorts, we identified the ECM pathway as the most common pathway among 7 pathways (**Figure 1B, C**). The relationship between Alzheimer's disease and the ECM has recently been recognized as a new molecular pathogenesis, along with other major pathological hypotheses[26,27]. ECM components contain

87 glycoproteins including glycosylated proteoglycans, collagen as one of major elements[27], and
88 many glycosylation have important roles in ECM formation and maintenance.
89
90 **Meta-analysis of the transcriptome reveals that glycogenes are enriched in the ECM**
91 We explore upstream factors that regulate ECM hyperglycosylation in AD. We
92 accessed the AD Knowledge Portal (https://adknowledgeportal.synapse.org), which contains
93 postmortem brain transcriptome data from multiple cohorts of Alzheimer's disease patients,
94 and compiled gene expression data. The glycogene set consisting of 214 glycosyltransferases
95 was defined by the gene list in the Glycogene Database (GGDB: https://acgg.asia/ggdb2/) [28]and
96 literature[6,29,30] (**Figure 2A, Supplementary Table 2**). This gene set is also categorized by
97 glycosylation pathway and synthesis step (**Figure 2A**).
98 We derived the transcriptional signatures of glycogenes based on meta-analysis. We
99 identified 46 differential expressed genes (DEGs) of glycogenes (**Figure 2B, Table S3**). We
100 mapped glycogenes to glycosylation pathways to determine which pathways are enriched for
101 DEGs (**Figure 2C**). In all pathways, glycosyltransferases were differentially expressed (**Figure**
102 **2C**), which implicates signals triggering aberrant glycosylation were already observed at the
103 transcriptional level.
104 Next, we analyzed the biological functions for these glycogene signatures. Globally
105 enriched 779 biological pathways were estimated based on the effect size from differential
106 expression obtained by meta-analysis using all genes (FDR < 5%) (**Figure 2D, Supplementary**
107 **Table S2 – S4**). Afterward, a post-hoc enrichment analysis was performed to infer which
108 glycosylation pathways are associated with these enriched biological pathways (**Figure 2D,**
109 **Supplementary Table S5**). The significant glycosylation pathways with hypergeometric test
110 were extracted as the final estimation results (**Figure 2D, Table S4-5; p-value < 5%**). We found
111 that the ECM is a common biological signature between layers of transcription and
112 glycosylation in AD (**Figure 3A**). The ECM cluster was strongly associated with the hydroxyl

113 galactose glycosylation pathway (**Figure 2D**).

114

115 **PLOD3 is identified as functional hub glycogene for ECM**

116 Next, we focused on an in-depth analysis of glycogenes that have a central role for
117 the ECM. Of the 779 globally enriched pathways, we constructed a bipartite graph consisting
118 of glycogene-pathway relationships based on 48 pathways including DEG glycogene (**Figure**
119 **3B**). We inferred glycogene importance via the number of neighboring pathways, i.e., network
120 degree (**Figure 3C**). As a result, Procollagen-Lysine,2-Oxoglutarate 5-Dioxygenase 3 (PLOD3)
121 was identified as hub glycogene with the highest degree (**Figure 3C**).

122 PLOD3 is an enzyme that mediates essential glycosylation in the early stages of
123 collagen formation[31]. In general, collagen is broadly modified by hydroxylation of proline and
124 lysine, and glycosylation of specific hydroxylysine (Hyl) residues[32]. Hydroxylation of lysine is
125 catalyzed by PLOD3[33,34] and hydroxyllysine undergoes further glycosylation and COLGALT1
126 transfers galactose, which are critical steps for maintaining collagen integrity[32].

127 To further confirm the results at the gene expression levels, we examined whether
128 expression changes of PLOD3 was consistent among the AD cohorts included in the meta-
129 analysis. We found that PLOD3 was consistently upregulated in individual cohort studies
130 (**Figure 3D**) and similarly, expression signatures of ECM organization and collagen formation
131 also showed a consistently overexpressed trend (**Figure 3D**). Based on this analysis, we
132 hypothesized that the hyperglycosylation of ECM in AD brain tissue is mediated by PLOD3.

133

134 **PLOD3 is expressed in oligodendrocytes and co-expressed with COL4A5**

135 We sought to determine the cellular origin of PLOD3 and collagen genes. First, we
136 accessed scRNA-seq data of normal brain tissue from the Human Protein Atlas (v22)[35,36]. We
137 found that PLOD3 exhibits a co-expression pattern with collagen type IV alpha 5 chain;
138 COL4A5 in oligodendrocytes (**Figure 4A**). These two genes showed distinct expression

139 signatures in an oligodendrocyte-specific manner (**Figure 4B**). We also accessed human AD
140 cohort of single-nucleus RNA-seq (snRNA-seq) data for the entorhinal cortex (GSE138852)[37].
141 The entorhinal cortex is one of the brain regions that shows neurodegeneration in the early
142 stages of AD[38–40]. The cohort included both non cognitive impairment (NCI) and AD brain.
143 There were six cell types: microglia, astrocytes, neurons, oligodendrocyte progenitor cells
144 (OPCs), oligodendrocytes, and endothelial cells (**Figure 4C**). PLOD3 and COL4A5 were highly
145 expressed in oligodendrocytes (**Figure 4C**). They also showed a tendency to be predominantly
146 expressed in the AD group cell population (**Figure 4C**).
147
148 **COL4A5 consistently correlated with amyloid fiber formation in multiple cohort studies**
149 COL4A5 has been partially reported to correlate with amyloid plaque accumulation[41].
150 However, it has not been validated in large clinical samples. We tested whether COL4A5
151 significantly correlates with Amyloid Beta Precursor Protein (APP) expression. We again
152 analyzed the bulk RNA-seq data used in the meta-analysis and examined the relationship
153 with APP gene expression, separately for each brain region in each study. The results showed
154 that COL4A5 strongly correlated with the APP gene in all datasets (**Figure 4D**). Furthermore,
155 we defined gene signatures of amyloid plaque formation pathway and analyzed the correlation
156 between their eigen gene expression and COL4A5 in the same way, and as expected, a strong
157 correlation was confirmed (**Figure 4D**). PLOD3 was evaluated similarly, showing a weaker
158 correlation than COL4A5, but significant in several data sets (**Supplementary Figure 1**).
159
160 **Cerebrovasculature most strongly associated with ECM dysregulation**
161 We explored whether overexpression of the PLOD3 - COL4A5 axis is involved in
162 biological processes in the AD brain. First, we analyzed the biological pathways that best
163 explain ECM activity. We used the AES-PCA[42–44], a principal component analysis (PCA)-based
164 regression model with ECM activity as the outcome variable and all other biological pathways'

165 activities as predictors for each AD cohort used in meta-analysis (**Figure 5A, Supplementary**
166 **Table S6**). The estimated p-values were statistically combined with fisher's method (**Figure**
167 **5A**). Four of the top 10 enriched genes were associated with the vascular system (**Figure 5A**)
168 and they were overexpressed molecules in the AD group at the expression level (**Figure 5B**).
169 We hypothesized that the PLOD3-COL4A5 axis is involved in the cerebrovascular
170 microenvironment.
171
172 **PLOD3 and COL4A5 expressed in oligodendrocytes of the cerebrovasculature**
173 **microenvironment**
174 We analyzed recently reported scRNA-seq data in the vascular microenvironment in
175 human brain (GSE16357)[45]. This data quantified gene expression by VINE-seq in cerebral
176 blood vessels in 8 NCI and 9 AD (**Figure 5C**). Gene expression was quantified in 143,793 cells
177 of 14 cell types, including vascular endothelial cells (arterial, capillary, and venous), mural
178 smooth muscle (SMC), pericytes, astrocytes, macrophages, T cells, perivascular and medullary
179 fibroblasts (**Figure 5C**). We examined cell types expressing PLOD3 and COL4A5, respectively.
180 They were found to be most strongly expressed in oligodendrocytes (**Figure 5D and 5E**). In
181 contrast, the other type 4 collagens were expressed mainly in pericytes and SMCs, consistent
182 with the fact that type 4 collagen constitutes the vascular basement membrane[46].
183
184 **Oligodendrocytes interact with astrocytes via COL4A5 ligand**
185 We next analyzed the biological functions and pathways mediated by the PLOD3-
186 COL4A5 axis in cerebrovasculature microenvironment. According to the KEGG pathway,
187 COL4A5 may contribute to cell-to-cell communication via ECM ligand receptors (hsa04512).
188 We analyzed how the PLOD3 - COL4A5 axis of oligodendrocytes mediates intercommunication
189 between cell types. CellChat[47] allows estimation of cell-cell interactions for each signaling
190 pathway. We estimated cell-cell interactions based on collagen signaling pathways in the AD

191 group. Oligodendrocyte interacted with astrocytes via COL4A5 ligand and CD44 receptor
192 (**Figure 6A**). It was also checked by NicheNet[48], another intercellular communication
193 estimation algorithm. In oligodendrocytes, COL4A5 was again identified as one of the most
194 promising candidates (**Figure 6B**). In addition to CD44 identified by CellChat, SDC4, DDR2,
195 ITGB8, and ITGAV were predicted as receptors in astrocytes (**Figure 6B**). These receptors
196 were highly expressed in astrocytes (**Figure 6C**).
197
198 **COL4A5 ligand is involved in the regulatory cascade of astrocyte stress response**
199 We further performed a detailed analysis of signaling pathways to understand the
200 biological functions of COL4A5-mediated interactions between oligodendrocytes and
201 astrocytes. We integrated the predicted COL4A5 ligand-receptor pairs (CD44, SDC4, DDR2,
202 ITGB8, ITGAV) onto prior knowledge of the signaling network constructed from multiple
203 perturbation experiments and databases with NicheNet. The results indicated COL4A5 ligand
204 can target and activate B-cell/CLL lymphoma 6 (BCL6) and Serum and glucocorticoid-
205 regulated kinase 1 (SGK1) via the ECM receptors in astrocytes (**Figure 6D**). BCL6 is a
206 transcription factor and is a known master regulator of humoral immunity and B-cell
207 lymphomagenesis, while SGK 1 encodes a serine/threonine protein kinase and plays an
208 important role in cellular stress responses[49–51]. Both of these genes were also found to be
209 expressed in astrocytes (**Figure 6E**).
210 Based on these results, we inferred the biological functions of gene modules with
211 BCL6 and SGK1 in astrocytes. An astrocyte-specific co-expression network was constructed
212 from gene expression using hdWGCNA algorithm[52] (**Figure 6F**). Next, we applied the random
213 walk with restart (RWR) algorithm[53], which is one of the network propagation algorithm,
214 starting from BCL6 and SGK1 on the astrocyte-specific network topology (**Figure 6F**). The
215 RWR allows the evaluation of the proximity on the network between BCL6 and SGK1 and
216 other neighboring genes. Based on the results, we prioritized top 30 neighbors (**Figure 6G**).

217 GO analysis on these neighbor gene groups revealed that they are enriched mainly for
218 processes involved in stress response (**Figure 6H**). These enriched pathways were also
219 observed in the GO analysis of BCL6 and SGK1, which were independently identified using
220 the network propagation method (**Supplementary Figure 3**).
221

222 **Discussion**

223 Our knowledge of how glycosylation, one of the major post-translational modifications,
224 is involved in the pathogenesis of Alzheimer's disease is lacking. We have systematically
225 explored pathogenesis and driving factors based on integrated analysis of emerging
226 dimensions of glycosylation in combination with transcriptomics.

227 In brain tissue from human Alzheimer's disease (AD) patients, hyperglycosylation in
228 the extracellular matrix (ECM) is the main signature shared by glycome and transcriptome,
229 and the glycosyltransferase Procollagen-Lysine,2-Oxoglutarate 5-Dioxygenase 3 (PLOD3) was
230 found to be an upstream regulator acting as a functional hub. PLOD3 was predominantly
231 expressed in oligodendrocytes in AD brain tissue and cerebrovasculature, and was co-
232 expressed with collagen type IV alpha 5 chain (COL4A5). Importantly, COL4A5 significantly
233 correlated with Amyloid Beta Precursor Protein (APP) and the activity of the amyloid fiber
234 formation pathway. Single-cell / nucleus analysis revealed that COL4A5 was a ligand for
235 oligodendrocytes that can mediate cell-cell interactions via ECM receptors on astrocytes.
236 Besides, signaling pathway network analysis identified BCL6 and SGK1 as its target genes
237 and their neighboring genes on the astrocyte-specific network analysis revealed that these two
238 genes are involved in the regulation of stress response.

239 The involvement of the ECM in Alzheimer's disease has been supported by a large
240 amount of literature[27,54–58]. The physiological roles of the ECM are diverse and include
241 developmental regulation, tissue homeostasis, cell migration, cell proliferation, cell
242 differentiation, neuronal plasticity, and neurite growth[59]. In AD, in particular, it is known to

243 be extensively involved in perineuronal network (PNN) dysregulation[58,60–68], which is involved
244 in maintaining spatial structure, neuronal plasticity, scaffolding[69] and promoting or inhibiting
245 aggregation, as well as in amyloid protein[27,70–75] and the brain-blood barrier (BBB) [41,54,76–79].
246 As glycoproteins are one of the major components of the ECM[55,59,80], the glycan synthesis is
247 clearly important for ECM homeostasis in brain. The enrichment of dysregulated
248 glycoproteins in the ECM is natural in this sense (**Figure 1A, B**).

249 We discovered that PLOD3 was enriched for ECM, and it was the up-regulated in AD
250 meta-analysis (**Figures 2B-D**). PLOD3 is known as a multifunctional enzyme, and in addition
251 to its role as a lysyl hydroxylase, it also functions as a collagen galactosyltransferase and
252 glucosyltransferase activity[34,81–83]. Although no direct evidence of PLOD3 in AD has been
253 reported, it is known to play an essential role in the formation of collagen, a major component
254 of the ECM[84]. For instance, defects in PLOD3 (or Lysyl hydroxylase 3; LH3) have been
255 implicated in causing inherited connective tissue disorders and have been shown to cause
256 cerebral small vessel injury[85,86], maintenance of the structural integrity of cerebral blood
257 vessels, regulating inflammatory processes[87]. This enzyme is also a promising biomarker in
258 AD, since its expression has been reported to fluctuate in cell-free RNA expression using blood
259 samples from AD patients[88].

260 PLOD3 mediates essential glycosylation during early collagen formation[31]. Type 4
261 collagen is an essential protein in the cerebral vasculature in Alzheimer's disease and is
262 responsible for network formation in the basement membrane. Indeed, in our analysis of
263 single-cell expression levels in cerebral vessels, many type 4 collagens
264 (COL4A1/COL4A2/COL4A3/COL4A4) were predominantly expressed in pericytes and SMCs
265 (**Figure 5E**). On the other hand, COL4A5 behaved differently from other type 4 collagens and
266 was expressed dominantly in oligodendrocytes. Oligodendrocytes have been shown to stably
267 bind to cerebral blood vessels by zonation analysis based on single cell / nucleus sequencing
268 analysis[89,90] and electron microscopy[91] . Interestingly, data from multiple studies supported

269 that COL4A5 strongly correlates with APP and amyloid fiber formation activity (**Figure 4D**),
270 suggesting a relationship with amyloid plaque accumulation. This may be relevant because
271 overexpression of type 4 collagen generally leads to an increase in cortical basement
272 membrane thickness and has been implicated in the degeneration of cerebral vascular
273 structures[55]. The functional role of type 4 collagen in AD cerebrovasculature needs to be
274 examined in detail by future studies.

275 We also performed in silico analysis of cell-cell interactions. COL4A5 functioned as a
276 ligand in oligodendrocyte-astrocyte interactions (**Figure 6A**). Analysis of the signaling
277 pathway network suggested that this cell-cell interaction may contribute primarily to the
278 stress response via SGK1 or BCL6 (**Figure 6D-H**). SGK1 is known to be transcriptionally
279 upregulated by cellular stress[49–51]. On the other hand, both factors have also been reported to
280 be involved in inflammatory responses in the central nervous system. Recent studies have
281 shown that the inhibition of SGK1 can suppress the NFκB-mediated inflammatory pathway
282 in glial cells[92]. There is also evidence that BCL6 plays a central role in astrocytes and NF-κB
283 in response to inflammatory stimuli and disorders[93]. Indeed, in our analysis of glycoproteins,
284 it was the immune response pathway that was enriched next to the ECM (**Figure 1B, C**), and
285 also significantly associated with the ECM organization pathway at the transcriptome level
286 were inflammatory cytokines (**Figure 5A and Supplementary Figure S2A**). Clearly,
287 inflammatory pathways can be characterized as key signatures in the AD brain, but their
288 mechanisms of action on the stress response remain unclear. Further examination of the
289 mechanisms of BCL6- and SGK1-mediated stress responses would be needed.

290 Several limitations of this study are described. The first is that the AD glycomics
291 analysis is limited to N-type glycans. Therefore, evidence of hyperglycosylation for ECM
292 should be verified by future studies using comprehensive glycomics data. Second, the AD
293 cohort data used in the meta-analysis was limited to data deposited in AD-knowledge portal.
294 In order to establish a higher level of evidence, data from other large cohort studies should be

295 included in the analysis. Third, single-cell sequencing data are collected from several different
296 data sources, so there is no guarantee that the results necessarily reflect the differential
297 expression results of the bulk sequencing used in the meta-analysis. It is expected that this
298 limitation can be overcome in the future as multilayered omics data are collected, but
299 validation including experimental approaches is needed.

300 Our results suggest that glycosylation is significantly involved in the pathogenesis
301 of AD in several as yet unclarified mechanisms. Our results also indicate that glycogenomics
302 analysis integrating genetic approaches is a promising method to highlight the biological
303 functions of glycans and the molecular pathogenesis of diseases at single-cell resolution.
304 Data on AD glycomics in human subjects are very limited. However, as glycomics analysis
305 technology matures, it is being applied to various disease areas, and a vast amount of
306 glycomics data will be accumulated in the next decade. The glycogenomics approach will
307 play an important role as a bridge between the established AD genetic pathology and the
308 new dimensional omics' piece, glycomics, in the near future.

**Figure 1. Hyperglycosylated proteins are primarily enriched in the extracellular matrix**. (A) Analysis of glycoprotein data from two AD cohorts, using glycoproteins from prefrontal tissues of two independent AD cohorts. The first cohort (AD cohort 1) consisted of 8 samples each from healthy subjects and AD, and the second cohort (AD cohort 2) consisted of 10 samples each from healthy subjects, asymptomatic, and symptomatic AD. In each cohort, 92 and 10 AD-specific glycoproteins were identified. (B) Pathway enrichment of AD-related glycoproteins. Over-representation analysis of AD-specific glycoproteins was performed. (C) Significantly enriched pathways that were common in both cohorts are shown. The horizontal axis is the p-value representing the enrichment, which is the logarithm of the nominal p-value multiplied by a negative value. Figures were created with BioRender.com.

323

324 **Figure 2. Meta-analysis of the global transcriptome reveals that glycogenes are enriched in the ECM.** (A)
325 Number of glycogenes constituting the glycosylation pathway used for transcriptome analysis. (B) Meta-
326 analysis of differential gene expression in multiple AD cohorts. transcriptome data from three AD cohorts:
327 the Mayo cohort (n=313), the MSSM cohort (n=315) and the ROSMAP cohort (n=1168). A meta-analysis of
328 Differential Expressed Gene (DEG) based on gene-level expression levels (FDR < 5%) was performed; 46
329 glycogenes were identified as DEGs. In the volcano plot, the horizontal axis represents the effect size
330 summarizing the difference in expression between the non-AD and AD groups across cohorts, and the
331 vertical axis represents the log of the p-value from the meta-analysis (bottom is 10) multiplied by a negative
332 value. (C) Mapped glycosyltransferase DEGs. 46 glycogene DEGs were mapped. Genes overexpressed in the
333 meta-analysis are shown in red, genes underexpressed are shown in blue, and genes that did not show
334 significant mutations are shown in gray. Genes are classified into 16 major glycosylation pathways:
335 initiation, core elongation, elongation/branching, capping, and sulfation. Glycosyltransferases with and
336 without pathway specificity are also distinguished. Figure created by BioRender.com.
337

338

339 **Figure 3. PLOD3 is identified as hub glycogene for ECM.** (A) Comparison of AD trascriptome and
340 glycoprotein signatures. Common pathways were shown. (B) Relationship between glycogenes and global
341 enriched pathways. Orange nodes represent globally enriched pathways and green nodes represent glycogen
342 enriched in each pathway. (C) Functional hub glycogenes in globally enriched pathways. To identify
343 functional hub glycogenes involved in multiple pathways, we constructed a pathway-gene bipartite graph,
344 calculated the degree of each glycogene (number of genes directly connected to the pathway), and ranked the
345 importance of each glycogene. The vertical axis of the bar graph represents the order of each glycogene. (D)
346 Activity changes of PLOD3, ECM and collagen formation in AD brains in each transcriptome cohort. Forest
347 plots of log 2-fold changes in PLOD3, ECM organization and collagen formation activity between non-AD
348 and AD are plotted by cohort and brain region. DLPFC stands for dorsolateral prefrontal cortex, STG for
349 superior temporal gyrus, PHG for parahippocampal gyrus, IFG for inferior frontal gyrus, and FP for frontal
350 pole, TCX represents temporal cortex, and CBE represents cerebellum. Dots indicate estimated mean effect
351 sizes, bar widths are 95% confidence intervals of the estimates, and vertical lines with red dots indicate zero
352 (no change).

353

354

355

356 **Figure 4. PLOD3 is expressed in oligodendrocytes and co-expressed with COL4A5**. (A) Cell type specificity
357 of PLOD3 in healthy brain tissues. Cell clusters obtained from gene expression in healthy brain tissue by
358 Human Protein Atlas (v22) scRNA-seq and the Transcript Per Million (TPM) in each cluster. PLOD3 and
359 COL4A5 are highly expressed in oligodendrocytes and belong to the same cluster. (B) Expression levels of
360 PLOD3 and COL4A5 per cell type. (C) Cellular specificity of PLOD3 and collagen in the enthorhinal cortex.
361 Scatter plots show the cluster structure of cell populations projected by UMAP to 2D coordinates based on
362 gene expression; the first panel shows cell types, the second non-AD and AD; the third and fourth panels
363 show cell type-specific expression of PLOD3 and COL4A5 in oligodendrocytes. (D) Correlation of COL4A5
364 with expression of APP (upper panel) and activity of amyloid fiber formation (lower panel) for each cohort
365 and each region. DLPFC stands for dorsolateral prefrontal cortex, STG for superior temporal gyrus, PHG
366 for parahippocampal gyrus, IFG for inferior frontal gyrus, and FP for frontal pole, TCX represents temporal
367 cortex, and CBE represents cerebellum.
368

369

370 **Figure 5. Cerebrovasculature most strongly associated with ECM dysregulation** (A) Pathways significantly
371 associated with the activity of the ECM organization were estimated for each cohort tissue using the AES-
372 PCA model. The p-values estimated for each cohort and for each brain tissue were estimated as integrated p-
373 values, and the top 10 pathways are shown in the figure. Figures were generated by BioRender.com. (B)
374 Enrichment of pathways involving the cerebrovasculature in AD with GSEA (FDR < 5%). Forest plots shown
375 below each enrichment plot indicate Log2 fold change for each pathway in each cohort and each region.
376 DLPFC stands for dorsolateral prefrontal cortex, STG for superior temporal gyrus, PHG for parahippocampal
377 gyrus, IFG for inferior frontal gyrus, and FP for frontal pole, TCX represents temporal cortex, and CBE
378 represents cerebellum. (C) Analysis using cerebrovascular scRNA-seq data (8NCI, 9AD). (D) Expression of
379 PLOD3 per cell type (E) Expression of type 4 collagen per cell type.

380

381

**Figure 6. COL4A5 ligand is involved in the regulatory cascade of astrocyte stress response.** (A) Estimated cell-to-cell communication based on ECM ligand - receptor expression (B) Receptor candidates for oligodendrocyte-derived COL4A5 ligands predicted to bind in astrocytes. (C) Cell type-specific expression levels of receptors for COL4A5. (D) COL4A5-mediated signaling pathways and target genes in astrocytes. (E) Expression levels of target genes BCL6 and SGK1 per cell type. (F) Analysis flow of the exploration of neighboring genes and functional estimation using network propagation in astrocyte-specific co-expression networks. (G) Top 30 neighboring genes estimated by network propagation based on BCL6 and SGK1. (H) Gene set analysis of BCL6 and SGK1 neighbor genes.

393

394 **Supplementary Figure 1.** Correlation of PLOD3 with activity of APP (upper panel) and
395 amyloid fiber formation (lower panel) for each cohort and each region. DLPFC stands for
396 dorsolateral prefrontal cortex, STG for superior temporal gyrus, PHG for parahippocampal
397 gyrus, IFG for inferior frontal gyrus, and FP for frontal pole, TCX represents temporal cortex,
398 and CBE represents cerebellum.

399

400

401 **Supplementary Figure 2. ECM activity is strongly associated with inflammatory cytokines.**
402 (A) Enrichment of pathways involving the immune system in AD with GSEA (FDR < 5%).
403 Forest plots shown below each enrichment plot indicate Log2 fold change for each pathway in
404 each cohort and each tissue. (B) Pathways significantly associated with ECM activity obtained
405 by applying AES-PCA for each cohort and region. DLPFC stands for dorsolateral prefrontal
406 cortex, STG for superior temporal gyrus, PHG for parahippocampal gyrus, IFG for inferior
407 frontal gyrus, and FP for frontal pole, TCX represents temporal cortex, and CBE represents
408 cerebellum.

409

410

**Supplementary Figure 3. COL4A5 ligand is involved in the regulatory cascade of astrocyte stress response.** (A) Top 30 neighboring genes estimated by network propagation based on BCL6. (B) Gene set analysis of BCL6 neighbor genes. (C) Top 30 neighboring genes estimated by network propagation based on SGK1. (B) Gene set analysis of SGK1 neighbor genes.

418 **Methods**

419 **Dataset compilation**

420 The Glycomics datasets were compiled and used from supplementary files published in the
421 respective papers[9,10]. For the AMP-AD transcriptome dataset, the data were obtained from
422 The RNAseq Harmonization Study (RNAseq Harmonization) repository (syn21241740).
423 Single-cell transcriptome data in the entorhinal cortex were obtained from GSE138852. Data
424 on the brain vascular were downloaded from GSE163577.
425

426 **Glycoproteomics enrichment analysis**

427 The first glycomics data[9], was analyzed for glycoproteins overexpressed in the AD group
428 (BRAAK ≥ 5) and the normal group (BRAAK ≤ 2), as defined in the original paper, using the
429 canonical pathway collection of MSigDB (c2.cp.v2022.1 Hs.symbols.gmt) were used for
430 enrichment analysis. All genes were analyzed as background using the fedup package in R
431 and the top 30 significantly enriched pathways were identified. The second glycomics data[9]
432 was analyzed in the same manner. Comparisons were made between the symptomatic group
433 (BRAAK ≥ 5 and CERAD 1 or 2), the asymptomatic group (BRAAK ≥ 3 and CERAD 1 or 2),
434 and the normal group (BRAAK ≤ 2 and CERAD 4) as defined in the original paper,
435 glycoproteins specifically identified in the symptomatic group were extracted. Enrichment
436 analysis was then performed to identify the top 30 significantly enriched pathways.
437

438 **Meta-Analysis**

439 Meta-analysis using RNAseq Harmonization of AMP-AD followed the published AD-
440 CONTROL analysis protocol (https://github.com/th1vairam/ampad-DiffExp/tree/df3efa793f
441 379730bae6d4c9e62910fb2c37e525/gene_level_analysis). First, meta-information was used
442 for data from three cohorts (ROSMAP, MSSM, and MAYO) including seven different brain
443 regions to define patients with definitive late-onset Alzheimer's disease from a clinical and
444 neuropathological perspective, that is, neurofibrillary changes, neuritic amyloid plaques, and
445 cognitive dysfunction The AD control group consisted of patients with AD.
446 AD controls were defined as patients with few plaques and neurofibrillary changes
447 and no cognitive impairment; in ROSMAP, LOAD cases were those with a BRAAK of 4 or more,
448 a CERAD score of 2 or less, and a cognitive diagnosis of probable AD with no other causes
449 (cogdx=4), LOAD controls are those with a BRAAK of 3 or less, a CERAD score of 3 or more,
450 and a cognitive diagnosis of "no cognitive impairment" (cogdx=1). For MSBB, LOAD cases
451 were defined as those with a CDR score of at least 1, a BRAAK score of at least 4, and a
452 CERAD score of at least 2. LOAD cases were similarly defined as those with a CDR score of
453 0.5 or less, a BRAAK of 3 or less, and a CERAD of 1 or less as LOAD controls. In Mayo, cases
454 were defined based on neuropathology, with LOAD cases defined as having a BRAAK score of
455 4 or higher, whereas LOAD controls were defined as having a BRAAK of 3 or lower.

A meta-analysis using a mixed-effects model was then performed on the differences in expression levels in each gene for each of the seven brain regions in each cohort. Effect sizes were estimated by restricted maximum likelihood (REML) based on standard mean difference (SMD) by Hedge. The metacont function from the meta package of the R language was used for the analysis. p-values were corrected for multiple testing by "fdr" using the p.adjust function from the stats package.

**Enrichment Map**

Gene Set Enrichment Analysis (GSEA) was performed on all genes included in the meta-analysis. The gene set was c2.cp.v2022.1.Hs.symbols from the MsigDB collection, which was loaded using Enrichment Map in Cytoscape and drawn with default settings. After drawing, we manually classified the pathways into several categories and drew several clusters on the network. The list of glycan-related genes manually defined for each glycosylation pathway was then analyzed by post hoc analysis using the Hyper Geometric Test and the Wilcoxon test, and pathways with FDR ≤ 5% and significant by two tests were extracted. The pathways that were significant by the two tests were extracted.

**Functional hub glycogene identification**

Among the pathways enriched based on the same GSEA results as the Enrichment Map, only pathways containing glycogenes were extracted, and from these, a two-part graph of pathway - glycogene was extracted. Based on the obtained two-part graphs, each gene was ranked based on its degree. The glycogene with the largest degree was defined as the functional hub glycogene. The results of querying the extracted PLOD3 to the String database (v11) are shown in Figure 2D. forest plots of PLOD3 was shown with estimated effect sizes and 95% confidence intervals from the meta-analysis. For pathway activity, GSEA was performed using the R fgsea package with gene ranks for effect sizes for each cohort and c2.cp.v2022.1.Hs.symbols for the gene set, and its Normalized Enrichment Score (NES) was used to forest plots were drawn.

**Cell type specificity of PLOD3**

For cell type specificity of healthy tissues, information was obtained from the Human Proteome Atalas (V22) website by entering the gene name. For data on entorhinal cortex, information was obtained by entering gene names from (http://adsn.ddnetbio.com/).

**Pathway-based PCA regression and GSEA**

Pathway-based PCA is a principal component analysis (PCA)-based method of analyzing pathways and phenotypic associations[43,44,94]. The R Bioconductor PathwayPCA package[42] was used. Using region-specific gene expression data from each AD cohort (MAYO, MSSM,

494 and ROSMAP), we specified the mean expression levels of the component genes of the ECM
495 pathway as ECM pathway activity for the objective variable and each pathway other than
496 the ECM pathway for the explanatory variables. The gene set used was
497 c2.cp.v2022.1.Hs.symbols from MSigDB. The pathway names containing "ECM,"
498 "Extracellular," or "Collagen" were defined as ECM pathways. The genes included in the
499 pathways were defined as signatures.
500 The p-values of the list of pathways significantly associated with ECM were
501 combined by Fisher's method to calculate an integrated p-value. For the calculation, the
502 logsum function of the R metapackage[95] was used and the p-values of the individual data
503 sets were entered for each pathway. In addition, we cross-checked whether significantly
504 related pathways were also sufficiently enriched at the expression level. Focusing on the top
505 10 pathways, we applied GSEA based on the gene set c2.cp.v2022.1.Hs.symbols from
506 MSigDB using the effect sizes of the 3 cohort meta-analysis as gene rank. To further validate
507 that the top 10 pathway activities tended to increase by cohort and region, the means of
508 effect sizes and confidence intervals were calculated for the signature genes and illustrated
509 as forest plots.
510
511 **Analysis of brain vascular with scRNA-seq**
512 The count data were preprocessed using the Seurat package in R. The data were pre-
513 processed using the Seurat package in R. That is, normalization, feature selection with vst,
514 scaling, and Dimensional reduction with PCA and UMAP were performed. Cell types were
515 visualized using those already identified in the original paper[45]. Next, for each cell type,
516 variation analysis among AD and cognitively normal groups was performed with Seurat's
517 FindMarkes function, and enrichment analysis for the identified groups of differentially
518 expressed genes was performed with R fedup package. The c2.cp.v2022.1.Hs.symbols from
519 MSigDB was used as the gene set to determine which cell types were enriched for ECM-
520 related pathways. We selected gene sets with pathway names containing "ECM,"
521 "Extracellular," "Matrisome," or "Collagen " in the pathway name. The enriched p-values
522 were further transformed as -log10(FDR) from the multiple-test-corrected FDR and were
523 considered as differentially expressed activity signals and visualized by heatmap. The
524 expression levels per cell type were obtained by querying (https://twc-
525 stanford.shinyapps.io/human_bbb/) for PLOD3.
526
527 **Cell-cell interaction and signaling network analysis**
528 Cell-cell interactions were analyzed using the R package CellChat[47]
529 (https://github.com/sqjin/CellChat). Oligodendrocytes - astrocytes identified with CellChat
530 were further analyzed using another algorithm, NicheNet[48] (https://
531 github.com/saeyslab/nichenetr) was used for analysis. For detailed analysis, the ligand-

receptor prior information was input by integrating the ligand-receptor pair information used in CellChat with the ligand-receptor pair information used in NicheNet. It was also used for the signal network analysis. A pre-built model was downloaded (https://github.com/saeyslab/nichenetr/blob/master/vignettes/model_construction.md) and the ligand-receptor information identified in the cell-cell interactions and the expression information identified in cell-cell interactions.

**Astrocyte cell type specific network propagation**

For astrocyte-specific network construction using cerebrovascular scRNA-seq, Toplogical Over lap Measure (TOM) was estimated using hdWGCNA[52], and edges were further defined only if they had a TOM above the 90th percentile as a threshold. The network propagation method was then applied using the R package RandomWalkRestartMH[53]. That is, we performed a random walk restart starting from SGK1 and BCL6 on the obtained network topology. The 30 most relevant neighbors were narrowed down and plotted using the R package igraph. The R package fedup (https://github.com/rosscm/fedup) was used for enrichment analysis. To estimate the transcriptional activity of BCL6, curated regulon information was first obtained using R package DoRothEA[96], and transcription factor target genes were estimated using the Viper[97] algorithm. R package decoupleR[98] was used for the analysis.

**Acknowledgement**

This work was supported by the Human Glycome Atlas Project (HGA) and JSPS KAKENHI Grant Number JP20H04282. The results published here are in part based on data obtained from the AD Knowledge Portal (https://adknowledgeportal.org). Data generation was supported by the following NIH grants: P30AG10161, P30AG72975, R01AG15819, R01AG17917, R01AG036836, U01AG46152, U01AG61356, U01AG046139, P50 AG016574, R01 AG032990, U01AG046139, R01AG018023, U01AG006576, U01AG006786, R01AG025711, R01AG017216, R01AG003949, R01NS080820, U24NS072026, P30AG19610, U01AG046170, RF1AG057440, and U24AG061340, and the Cure PSP, Mayo and Michael J Fox foundations, Arizona Department of Health Services and the Arizona Biomedical Research Commission. We thank the participants of the Religious Order Study and Memory and Aging projects for the generous donation, the Sun Health Research Institute Brain and Body Donation Program, the Mayo Clinic Brain Bank, and the Mount Sinai/JJ Peters VA Medical Center NIH Brain and Tissue Repository. Data and analysis contributing investigators include Nilüfer Ertekin-Taner, Steven Younkin (Mayo Clinic, Jacksonville, FL), Todd Golde (University of Florida), Nathan Price (Institute for Systems Biology), David Bennett, Christopher Gaiteri (Rush University), Philip De Jager (Columbia University), Bin Zhang, Eric Schadt, Michelle Ehrlich, Vahram Haroutunian, Sam Gandy (Icahn School of

Medicine at Mount Sinai), Koichi Iijima (National Center for Geriatrics and Gerontology, Japan), Scott Noggle (New York Stem Cell Foundation), Lara Mangravite (Sage Bionetworks).

573 **Refences**


574 1. Guerreiro, R. & Bras, J. The age factor in Alzheimer's disease. *Genome Med.* **7**, 106 (2015).

575 2. Xia, X., Jiang, Q., McDermott, J. & Han, J.-D. J. Aging and Alzheimer's disease:

576 Comparison and associations from molecular to system level. *Aging Cell* **17**, e12802 (2018).

577 3. Breijyeh, Z. & Karaman, R. Comprehensive Review on Alzheimer's Disease: Causes and

578 Treatment. *Molecules* **25**, (2020).

579 4. Bennett, D. A. *et al.* Religious Orders Study and Rush Memory and Aging Project. *J.*

580 *Alzheimers. Dis.* **64**, S161–S189 (2018).

581 5. Gaunitz, S., Tjernberg, L. O. & Schedin-Weiss, S. What Can N-glycomics and N-

582 glycoproteomics of Cerebrospinal Fluid Tell Us about Alzheimer Disease? *Biomolecules*

583 **11**, 858 (2021).

584 6. Schjoldager, K. T., Narimatsu, Y., Joshi, H. J. & Clausen, H. Global view of human protein

585 glycosylation pathways and functions. *Nat. Rev. Mol. Cell Biol.* **21**, 729–749 (2020).

586 7. Narimatsu, Y. *et al.* An Atlas of Human Glycosylation Pathways Enables Display of the

587 Human Glycome by Gene Engineered Cells. *Mol. Cell* **75**, 394-407.e5 (2019).

588 8. Joshi, H. J. *et al.* Glycosyltransferase genes that cause monogenic congenital disorders of

589 glycosylation are distinct from glycosyltransferase genes associated with complex

590 diseases. *Glycobiology* **28**, 284–294 (2018).

591 9. Zhang, Q., Ma, C., Chin, L.-S. & Li, L. Integrative glycoproteomics reveals protein N-

592 glycosylation aberrations and glycoproteomic network alterations in Alzheimer's disease.

593 *Sci Adv* **6**, (2020).

594 10. Suttapitugsakul, S. *et al.* Glycoproteomics Landscape of Asymptomatic and Symptomatic

595 Human Alzheimer's Disease Brain. *Mol. Cell. Proteomics* **21**, 100433 (2022).

596 11. Yu, L. *et al.* Human Brain and Blood N-Glycome Profiling in Alzheimer's Disease and

597 Alzheimer's Disease-Related Dementias. *Front. Aging Neurosci.* **13**, 765259 (2021).

598 12. Kerdsaeng, N. *et al.* Serum Glycoproteomics and Identification of Potential Mechanisms

599 Underlying Alzheimer's Disease. *Behav. Neurol.* **2021**, 1434076 (2021).

600 13. Gizaw, S. T., Ohashi, T., Tanaka, M., Hinou, H. & Nishimura, S.-I. Glycoblotting method

601 allows for rapid and efficient glycome profiling of human Alzheimer's disease brain, serum

602 and cerebrospinal fluid towards potential biomarker discovery. *Biochim. Biophys. Acta*

603 **1860**, 1716–1727 (2016).

604 14. Gaunitz, S., Tjernberg, L. O. & Schedin-Weiss, S. The N-glycan profile in cortex and

605 hippocampus is altered in Alzheimer disease. *J. Neurochem.* **159**, 292–304 (2020).

606 15. Reyes, C. D. G. *et al.* LC-MS/MS Isomeric Profiling of N-Glycans Derived from Low-

607 Abundant Serum Glycoproteins in Mild Cognitive Impairment Patients. *Biomolecules* **12**,

608 (2022).

609 16. Frenkel-Pinter, M. *et al.* Interplay between protein glycosylation pathways in Alzheimer's

610 disease. *Sci Adv* **3**, e1601576 (2017).

611 17. Chen, C. C. *et al.* Altered serum glycomics in Alzheimer disease: a potential blood

612 biomarker? *Rejuvenation Res.* **13**, 439–444 (2010).

613 18. Schedin-Weiss, S. *et al.* Glycan biomarkers for Alzheimer disease correlate with T-tau and

614 P-tau in cerebrospinal fluid in subjective cognitive impairment. *FEBS J.* **287**, 3221–3234

615 (2020).

616 19. Palmigiano, A. *et al.* CSF N-glycoproteomics for early diagnosis in Alzheimer's disease. *J.*

617 *Proteomics* **131**, 29–37 (2015).

618 20. Cho, B. G., Veillon, L. & Mechref, Y. N-Glycan Profile of Cerebrospinal Fluids from

619 Alzheimer's Disease Patients Using Liquid Chromatography with Mass Spectrometry. *J.*

620 *Proteome Res.* **18**, 3770–3779 (2019).

621 21. Kizuka, Y. *et al.* An aberrant sugar modification of BACE1 blocks its lysosomal targeting

622 in Alzheimer's disease. *EMBO Mol. Med.* **7**, 175–189 (2015).

623 22. Kizuka, Y. *et al.* Bisecting GlcNAc modification stabilizes BACE1 protein under oxidative

624 stress conditions. *Biochem. J* **473**, 21–30 (2015).

625 23. Kizuka, Y., Kitazume, S., Sato, K. & Taniguchi, N. Clec4g (LSECtin) interacts with

626 BACE1 and suppresses Aβ generation. *FEBS Lett.* **589**, 1418–1422 (2015).

627 24. Bennun, S. V. *et al.* Systems Glycobiology: Integrating Glycogenomics, Glycoproteomics,

628 Glycomics, and Other 'Omics Data Sets to Characterize Cellular Glycosylation Processes.

629 *J. Mol. Biol.* **428**, 3337–3352 (2016).

630 25. West, C. M., Malzl, D., Hykollari, A. & Wilson, I. B. H. Glycomics, Glycoproteomics, and

631 Glycogenomics: An Inter-Taxa Evolutionary Perspective. *Mol. Cell. Proteomics* **20**, 100024
632 (2021).
633 26. Terry, A. V., Jr & Buccafusco, J. J. The cholinergic hypothesis of age and Alzheimer's
634 disease-related cognitive deficits: recent challenges and their implications for novel drug
635 development. *J. Pharmacol. Exp. Ther.* **306**, 821–827 (2003).
636 27. Sun, Y. *et al.* Role of the Extracellular Matrix in Alzheimer's Disease. *Front. Aging*
637 *Neurosci.* **13**, 707466 (2021).
638 28. Narimatsu, H. *et al.* GlycoGene Database (GGDB) on the Semantic Web. in *A Practical*
639 *Guide to Using Glycomics Databases* (ed. Aoki-Kinoshita, K. F.) 163–175 (Springer Japan,
640 2017).
641 29. Narimatsu, H. Construction of a human glycogene library and comprehensive functional
642 analysis. *Glycoconj. J.* **21**, 17–24 (2004).
643 30. *Handbook of Glycosyltransferases and Related Genes*. (Springer Japan).
644 31. Myllyharju, J. & Kivirikko, K. I. Collagens, modifying enzymes and their mutations in
645 humans, flies and worms. *Trends Genet.* **20**, 33–43 (2004).
646 32. Hennet, T. Collagen glycosylation. *Curr. Opin. Struct. Biol.* **56**, 131–138 (2019).
647 33. Heikkinen, J. *et al.* Lysyl Hydroxylase 3 Is a Multifunctional Protein Possessing Collagen
648 Glucosyltransferase Activity*. *J. Biol. Chem.* **275**, 36158–36163 (2000).
649 34. Wang, C. *et al.* The third activity for lysyl hydroxylase 3: galactosylation of hydroxylysyl

650 residues in collagens in vitro. *Matrix Biol.* **21**, 559–566 (2002).

651 35. Sjöstedt, E. *et al.* An atlas of the protein-coding genes in the human, pig, and mouse brain.

652 *Science* **367**, (2020).

653 36. Uhlén, M. *et al.* Proteomics. Tissue-based map of the human proteome. *Science* **347**,

654 1260419 (2015).

655 37. Grubman, A. *et al.* A single-cell atlas of entorhinal cortex from individuals with

656 Alzheimer's disease reveals cell-type-specific gene expression regulation. *Nat. Neurosci.*

657 **22**, 2087–2097 (2019).

658 38. Howett, D. *et al.* Differentiation of mild cognitive impairment using an entorhinal cortex-

659 based test of virtual reality navigation. *Brain* **142**, 1751–1766 (2019).

660 39. Khan, U. A. *et al.* Molecular drivers and cortical spread of lateral entorhinal cortex

661 dysfunction in preclinical Alzheimer's disease. *Nat. Neurosci.* **17**, 304–311 (2014).

662 40. Bottero, V., Powers, D., Yalamanchi, A., Quinn, J. P. & Potashkin, J. A. Key Disease

663 Mechanisms Linked to Alzheimer's Disease in the Entorhinal Cortex. *Int. J. Mol. Sci.* **22**,

664 (2021).

665 41. Lepelletier, F.-X., Mann, D. M. A., Robinson, A. C., Pinteaux, E. & Boutin, H. Early

666 changes in extracellular matrix in Alzheimer's disease. *Neuropathol. Appl. Neurobiol.* **43**,

667 167–182 (2015).

668 42. Odom, G. J. *et al.* PathwayPCA: An R/Bioconductor package for pathway based

669 integrative analysis of multi-omics data. *Proteomics* **20**, e1900409 (2020).

670 43. Chen, X., Wang, L., Smith, J. D. & Zhang, B. Supervised principal component analysis for
671 gene set enrichment of microarray data with continuous or survival outcomes.
672 *Bioinformatics* **24**, 2474–2481 (2008).

673 44. Chen, X. *et al.* Pathway-based analysis for genome-wide association studies using
674 supervised principal components. *Genet. Epidemiol.* **34**, 716–724 (2010).

675 45. Yang, A. C. *et al.* A human brain vascular atlas reveals diverse mediators of Alzheimer's
676 risk. *Nature* **603**, 885–892 (2022).

677 46. Xu, L., Nirwane, A. & Yao, Y. Basement membrane and blood-brain barrier. *Stroke Vasc*
678 *Neurol* **4**, 78–82 (2019).

679 47. Guerrero-Juarez, C. F. *et al.* Single-cell analysis reveals fibroblast heterogeneity and
680 myeloid-derived adipocyte progenitors in murine skin wounds. *Nat. Commun.* **10**, 650
681 (2019).

682 48. Browaeys, R., Saelens, W. & Saeys, Y. NicheNet: modeling intercellular communication
683 by linking ligands to target genes. *Nat. Methods* **17**, 159–162 (2020).

684 49. Lang, F., Stournaras, C., Zacharopoulou, N., Voelkl, J. & Alesutan, I. Serum- and
685 glucocorticoid-inducible kinase 1 and the response to cell stress. *Cell Stress Chaperones*
686 **3**, 1–8 (2018).

687 50. Leong, M. L. L., Maiyar, A. C., Kim, B., O'Keeffe, B. A. & Firestone, G. L. Expression of

the serum- and glucocorticoid-inducible protein kinase, Sgk, is a cell survival response to multiple types of environmental stress stimuli in mammary epithelial cells. *J. Biol. Chem.* **278**, 5871–5882 (2003).

51. Webster, M. K., Goya, L., Ge, Y., Maiyar, A. C. & Firestone, G. L. Characterization of sgk, a novel member of the serine/threonine protein kinase gene family which is transcriptionally induced by glucocorticoids and serum. *Mol. Cell. Biol.* **13**, 2031–2040 (1993).

52. Morabito, S., Reese, F., Rahimzadeh, N., Miyoshi, E. & Swarup, V. hdWGCNA identifies co-expression networks in high-dimensional transcriptomics data. *Cell Rep Methods* **3**, 100498 (2023).

53. Valdeolivas, A. *et al.* Random walk with restart on multiplex and heterogeneous biological networks. *Bioinformatics* **35**, 497–505 (2019).

54. Anwar, M. M., Özkan, E. & Gürsoy-Özdemir, Y. The role of extracellular matrix alterations in mediating astrocyte damage and pericyte dysfunction in Alzheimer's disease: A comprehensive review. *Eur. J. Neurosci.* **56**, 5453–5475 (2021).

55. Ma, J. *et al.* Extracellular Matrix Proteins Involved in Alzheimer's Disease. *Chemistry* **26**, 12101–12110 (2020).

56. Levy, A. D., Omar, M. H. & Koleske, A. J. Extracellular matrix control of dendritic spine and synapse structure and plasticity in adulthood. *Front. Neuroanat.* **8**, 116 (2014).

57. Morawski, M., Filippov, M., Tzinia, A., Tsilibary, E. & Vargova, L. ECM in brain aging and dementia. *Prog. Brain Res.* **214**, 207–227 (2014).

58. Soleman, S., Filippov, M. A., Dityatev, A. & Fawcett, J. W. Targeting the neural extracellular matrix in neurological disorders. *Neuroscience* **253**, 194–213 (2013).

59. Sethi, M. K. & Zaia, J. Extracellular matrix proteomics in schizophrenia and Alzheimer's disease. *Anal. Bioanal. Chem.* **409**, 379–394 (2016).

60. Bosiacki, M. *et al.* Perineuronal Nets and Their Role in Synaptic Homeostasis. *Int. J. Mol. Sci.* **20**, (2019).

61. Li, Y., Li, Z.-X., Jin, T., Wang, Z.-Y. & Zhao, P. Tau Pathology Promotes the Reorganization of the Extracellular Matrix and Inhibits the Formation of Perineuronal Nets by Regulating the Expression and the Distribution of Hyaluronic Acid Synthases. *J. Alzheimers. Dis.* **57**, 395–409 (2017).

62. Duncan, J. A., Foster, R. & Kwok, J. C. F. The potential of memory enhancement through modulation of perineuronal nets. *Br. J. Pharmacol.* **176**, 3611–3621 (2019).

63. Wen, T. H., Binder, D. K., Ethell, I. M. & Razak, K. A. The Perineuronal "Safety" Net? Perineuronal Net Abnormalities in Neurological Disorders. *Front. Mol. Neurosci.* **11**, 270 (2018).

64. Pantazopoulos, H. & Berretta, S. In Sickness and in Health: Perineuronal Nets and Synaptic Plasticity in Psychiatric Disorders. *Neural Plast.* **2016**, 9847696 (2015).

65. Logsdon, A. F. *et al.* Decoding perineuronal net glycan sulfation patterns in the Alzheimer's disease brain. *Alzheimers. Dement.* **18**, 942–954 (2021).

66. Miyata, S. & Kitagawa, H. Chondroitin sulfate and neuronal disorders. *Front. Biosci.* **21**, 1330–1340 (2016).

67. Galtrey, C. M. & Fawcett, J. W. The role of chondroitin sulfate proteoglycans in regeneration and plasticity in the central nervous system. *Brain Res. Rev.* **54**, 1–18 (2007).

68. Yamada, J. & Jinno, S. Spatio-temporal differences in perineuronal net expression in the mouse hippocampus, with reference to parvalbumin. *Neuroscience* **253**, 368–379 (2013).

69. Brandan, E. & Inestrosa, N. C. Extracellular matrix components and amyloid in neuritic plaques of Alzheimer's disease. *Gen. Pharmacol.* **24**, 1063–1068 (1993).

70. Zhang, S. *et al.* The extracellular matrix enriched with membrane metalloendopeptidase and insulin-degrading enzyme suppresses the deposition of amyloid-beta peptide in Alzheimer's disease cell models. *J. Tissue Eng. Regen. Med.* **13**, 1759–1769 (2019).

71. Wu, A., Pangalos, M. N., Efthimiopoulos, S., Shioi, J. & Robakis, N. K. Appican expression induces morphological changes in C6 glioma cells and promotes adhesion of neural cells to the extracellular matrix. *J. Neurosci.* **17**, 4987–4993 (1997).

72. Small, D. H., Nurcombe, V., Clarris, H., Beyreuther, K. & Masters, C. L. The role of extracellular matrix in the processing of the amyloid protein precursor of Alzheimer's disease. *Ann. N. Y. Acad. Sci.* **695**, 169–174 (1993).

73. Stoyanov, S. *et al.* Attenuation of the extracellular matrix restores microglial activity during the early stage of amyloidosis. *Glia* **69**, 182–200 (2020).

74. Bronfman, F. C., Soto, C., Tapia, L., Tapia, V. & Inestrosa, N. C. Extracellular matrix regulates the amount of the beta-amyloid precursor protein and its amyloidogenic fragments. *J. Cell. Physiol.* **166**, 360–369 (1996).

75. Salza, R., Lethias, C. & Ricard-Blum, S. The Multimerization State of the Amyloid-β42 Amyloid Peptide Governs its Interaction Network with the Extracellular Matrix. *J. Alzheimers. Dis.* **56**, 991–1005 (2017).

76. Potjewyd, G., Kellett, K. A. B. & Hooper, N. M. 3D hydrogel models of the neurovascular unit to investigate blood-brain barrier dysfunction. *Neuronal Signal* **5**, NS20210027 (2021).

77. Reed, M. J., Damodarasamy, M. & Banks, W. A. The extracellular matrix of the blood-brain barrier: structural and functional roles in health, aging, and Alzheimer's disease. *Tissue Barriers* **7**, 1651157 (2019).

78. Damodarasamy, M. *et al.* The microvascular extracellular matrix in brains with Alzheimer's disease neuropathologic change (ADNC) and cerebral amyloid angiopathy (CAA). *Fluids Barriers CNS* **17**, 60 (2020).

79. Brzdak, P., Nowak, D., Wiera, G. & Mozrzymas, J. W. Multifaceted Roles of Metzincins in CNS Physiology and Pathology: From Synaptic Plasticity and Cognition to

764 Neurodegenerative Disorders. *Front. Cell. Neurosci.* **11**, 178 (2017).

765 80. Bres, E. E. & Faissner, A. Low Density Receptor-Related Protein 1 Interactions With the

766 Extracellular Matrix: More Than Meets the Eye. *Front Cell Dev Biol* **7**, 31 (2019).

767 81. Wang, C. *et al.* The glycosyltransferase activities of lysyl hydroxylase 3 (LH3) in the

768 extracellular space are important for cell growth and viability. *J. Cell. Mol. Med.* **13**, 508–

769 521 (2009).

770 82. Salo, A. M. *et al.* Lysyl hydroxylase 3 (LH3) modifies proteins in the extracellular space,

771 a novel mechanism for matrix remodeling. *J. Cell. Physiol.* **207**, 644–653 (2006).

772 83. Valtavaara, M., Szpirer, C., Szpirer, J. & Myllylä, R. Primary Structure, Tissue

773 Distribution, and Chromosomal Localization of a Novel Isoform of Lysyl Hydroxylase

774 (Lysyl Hydroxylase 3)*. *J. Biol. Chem.* **273**, 12881–12886 (1998).

775 84. De Giorgi, F., Fumagalli, M., Scietti, L. & Forneris, F. Collagen hydroxylysine

776 glycosylation: non-conventional substrates for atypical glycosyltransferase enzymes.

777 *Biochem. Soc. Trans.* **49**, 855–866 (2021).

778 85. Zhou, J. *et al.* Cerebral small vessel disease caused by PLOD3 mutation: Expanding the

779 phenotypic spectrum of lysyl hydroxylase-3 deficiency. *Pediatr Investig* **6**, 219–223 (2022).

780 86. Miyatake, S. *et al.* Biallelic COLGALT1 variants are associated with cerebral small vessel

781 disease. *Ann. Neurol.* **84**, 843–853 (2018).

782 87. Li, H. *et al.* Overexpression of LH3 reduces the incidence of hypertensive intracerebral

783 hemorrhage in mice. *J. Cereb. Blood Flow Metab.* **39**, 547–561 (2019).

784 88. Toden, S. *et al.* Noninvasive characterization of Alzheimer's disease by circulating, cell-

785 free messenger RNA next-generation sequencing. *Sci Adv* **6**, (2020).

786 89. Garcia, F. J. *et al.* Single-cell dissection of the human brain vasculature. *Nature* **603**, 893–

787 899 (2022).

788 90. Vanlandewijck, M. *et al.* A molecular atlas of cell types and zonation in the brain

789 vasculature. *Nature* **554**, 475–480 (2018).

790 91. Palhol, J. S. C. *et al.* Direct association with the vascular basement membrane is a

791 frequent feature of myelinating oligodendrocytes in the neocortex. *Fluids Barriers CNS*

792 **20**, 24 (2023).

793 92. Kwon, O.-C. *et al.* SGK1 inhibition in glia ameliorates pathologies and symptoms in

794 Parkinson disease animal models. *EMBO Mol. Med.* **13**, e13076 (2021).

795 93. Linnerbauer, M., Wheeler, M. A. & Quintana, F. J. Astrocyte Crosstalk in CNS

796 Inflammation. *Neuron* **108**, 608–622 (2020).

797 94. Chen, X. Adaptive elastic-net sparse principal component analysis for pathway

798 association testing. *Stat. Appl. Genet. Mol. Biol.* **10**, (2011).

799 95. Dewey, M. Meta-Analysis of Significance Values [R package metap version 1.8]. (2022).

800 96. Garcia-Alonso, L., Holland, C. H., Ibrahim, M. M., Turei, D. & Saez-Rodriguez, J.

801 Benchmark and integration of resources for the estimation of human transcription factor

activities. *Genome Res.* **29**, 1363–1375 (2019).

97. Alvarez, M. J. *et al.* Functional characterization of somatic mutations in cancer using network-based inference of protein activity. *Nat. Genet.* **48**, 838–847 (2016).

98. Badia-I-Mompel, P. *et al.* decoupleR: ensemble of computational methods to infer biological activities from omics data. *Bioinform Adv* **2**, vbac016 (2022).

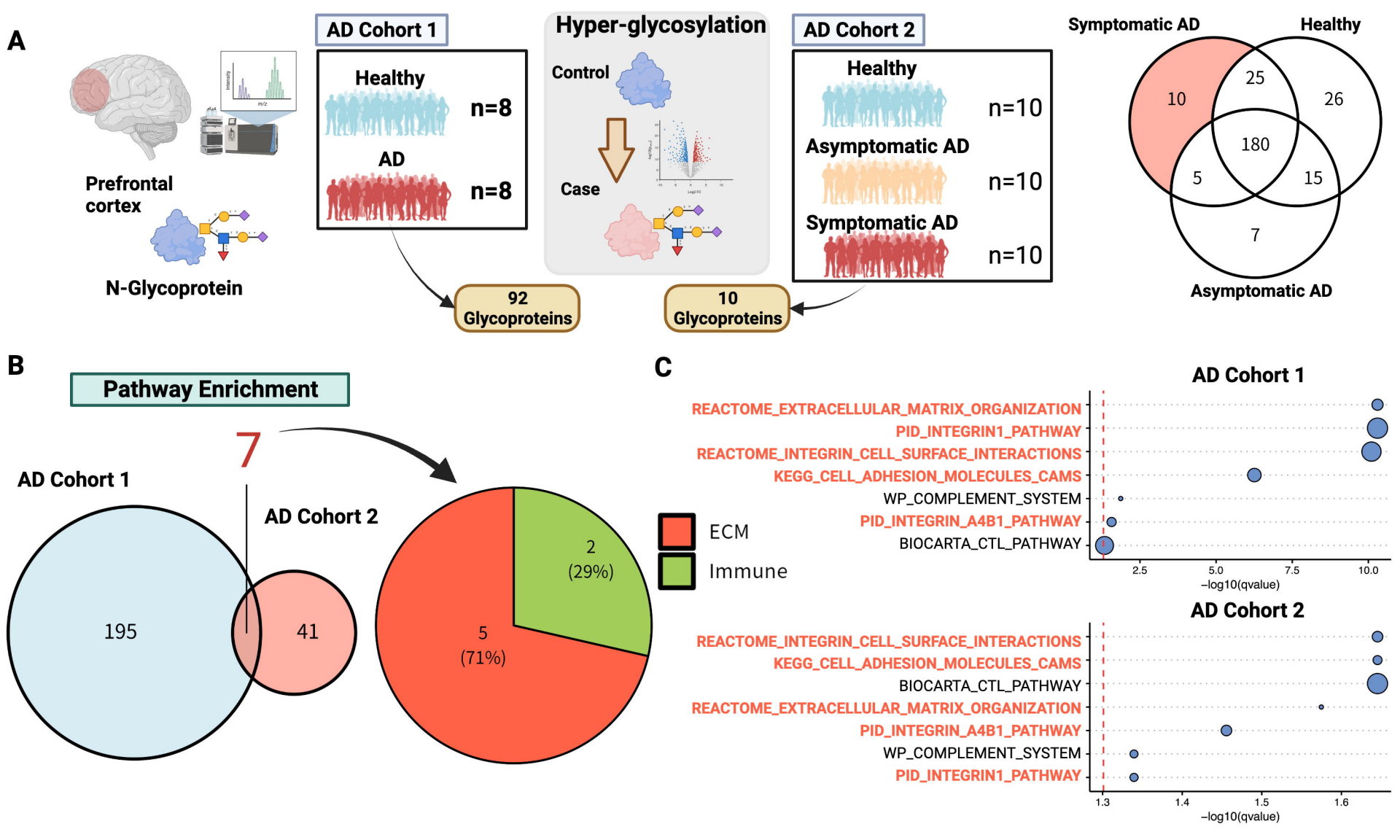
A
Prefrontal cortex
N-Glycoprotein
AD Cohort 1
Healthy
n=8
AD
n=8
Hyper-glycosylation
Control
Case
AD Cohort 2
Healthy
n=10
Asymptomatic AD
n=10
Symptomatic AD
n=10
92 Glycoproteins
10 Glycoproteins
Symptomatic AD
Healthy
Asymptomatic AD
10
25
26
180
5
15
7
B
Pathway Enrichment
7
AD Cohort 1
AD Cohort 2
195
41
5 (71%)
2 (29%)
ECM
Immune
C
AD Cohort 1
REACTOME_EXTRACELLULAR_MATRIX_ORGANIZATION
PID_INTEGRIN1_PATHWAY
REACTOME_INTEGRIN_CELL_SURFACE_INTERACTIONS
KEGG_CELL_ADHESION_MOLECULES_CAMS
WP_COMPLEMENT_SYSTEM
PID_INTEGRIN_A4B1_PATHWAY
BIOCARTA_CTL_PATHWAY
2.5
5.0
7.5
10.0
−log10(qvalue)
AD Cohort 2
REACTOME_INTEGRIN_CELL_SURFACE_INTERACTIONS
KEGG_CELL_ADHESION_MOLECULES_CAMS
BIOCARTA_CTL_PATHWAY
REACTOME_EXTRACELLULAR_MATRIX_ORGANIZATION
PID_INTEGRIN_A4B1_PATHWAY
WP_COMPLEMENT_SYSTEM
PID_INTEGRIN1_PATHWAY
1.3
1.4
1.5
1.6
−log10(qvalue)

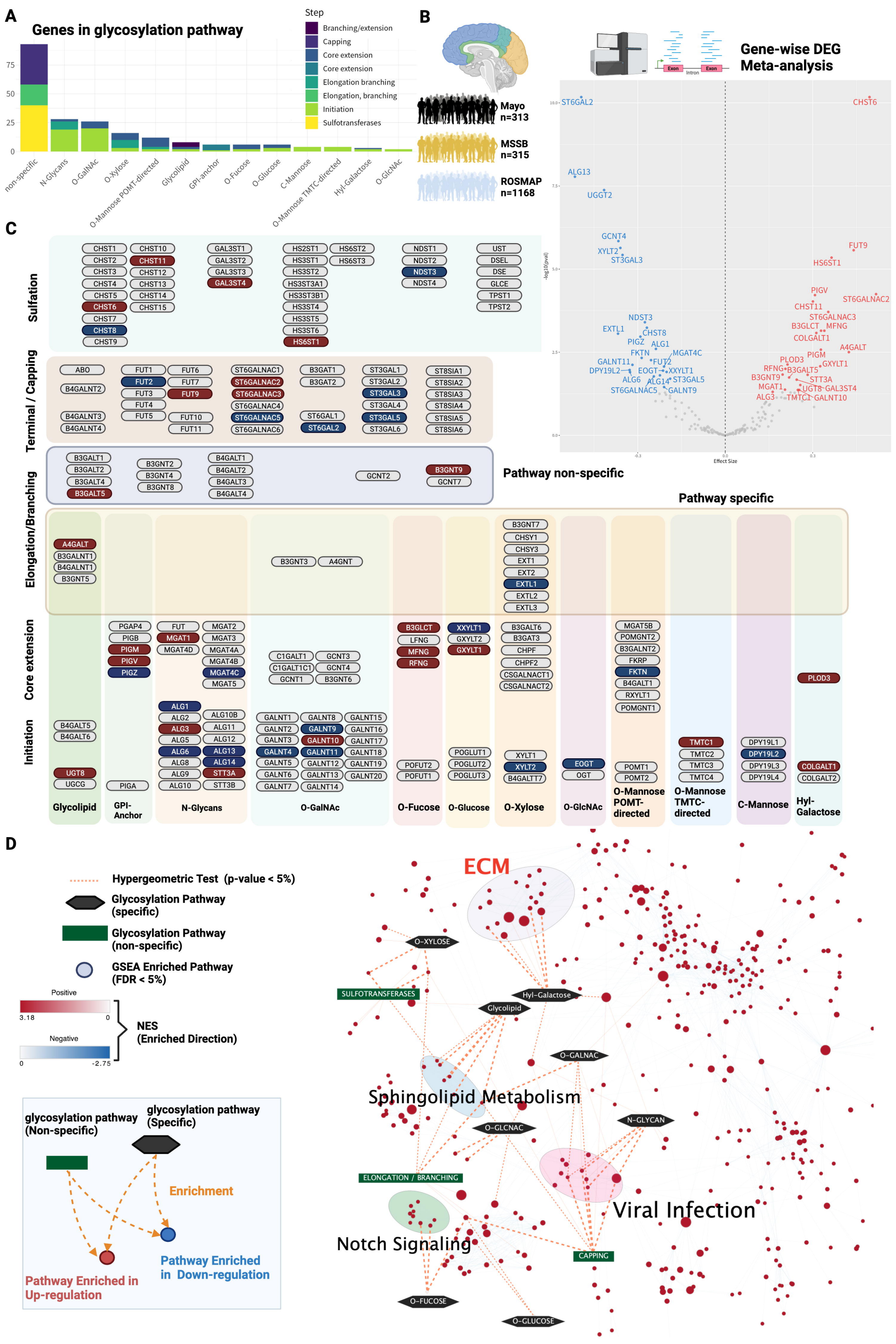
A
Genes in glycosylation pathway
Step
Branching/extension
Capping
Core extension
Core extension
Elongation branching
Elongation, branching
Initiation
Sulfotransferases
non-specific
N-Glycans
O-GalNAc
O-Xylose
O-Mannose POMT-directed
Glycolipid
GPI-anchor
O-Fucose
O-Glucose
C-Mannose
O-Mannose TMTC-directed
Hyl-Galactose
O-GlcNAc
B
Mayo n=313
MSSB n=315
ROSMAP n=1168
Gene-wise DEG Meta-analysis
Exon
Intron
Exon
-log10(pval)
Effect Size
C
Sulfation
Terminal / Capping
Elongation/Branching
Core extension
Initiation
Pathway non-specific
Pathway specific
Glycolipid
GPI-Anchor
N-Glycans
O-GalNAc
O-Fucose
O-Glucose
O-Xylose
O-GlcNAc
O-Mannose POMT-directed
O-Mannose TMTC-directed
C-Mannose
Hyl-Galactose
D
Hypergeometric Test (p-value < 5%)
Glycosylation Pathway (specific)
Glycosylation Pathway (non-specific)
GSEA Enriched Pathway (FDR < 5%)
Positive
3.18
0
Negative
0
-2.75
NES (Enriched Direction)
glycosylation pathway (Non-specific)
glycosylation pathway (Specific)
Enrichment
Pathway Enriched in Down-regulation
Pathway Enriched in Up-regulation
ECM
O-XYLOSE
SULFOTRANSFERASES
Hyl-Galactose
Glycolipid
O-GALNAC
Sphingolipid Metabolism
O-GLCNAC
N-GLYCAN
ELONGATION / BRANCHING
Viral Infection
Notch Signaling
CAPPING
O-FUCOSE
O-GLUCOSE

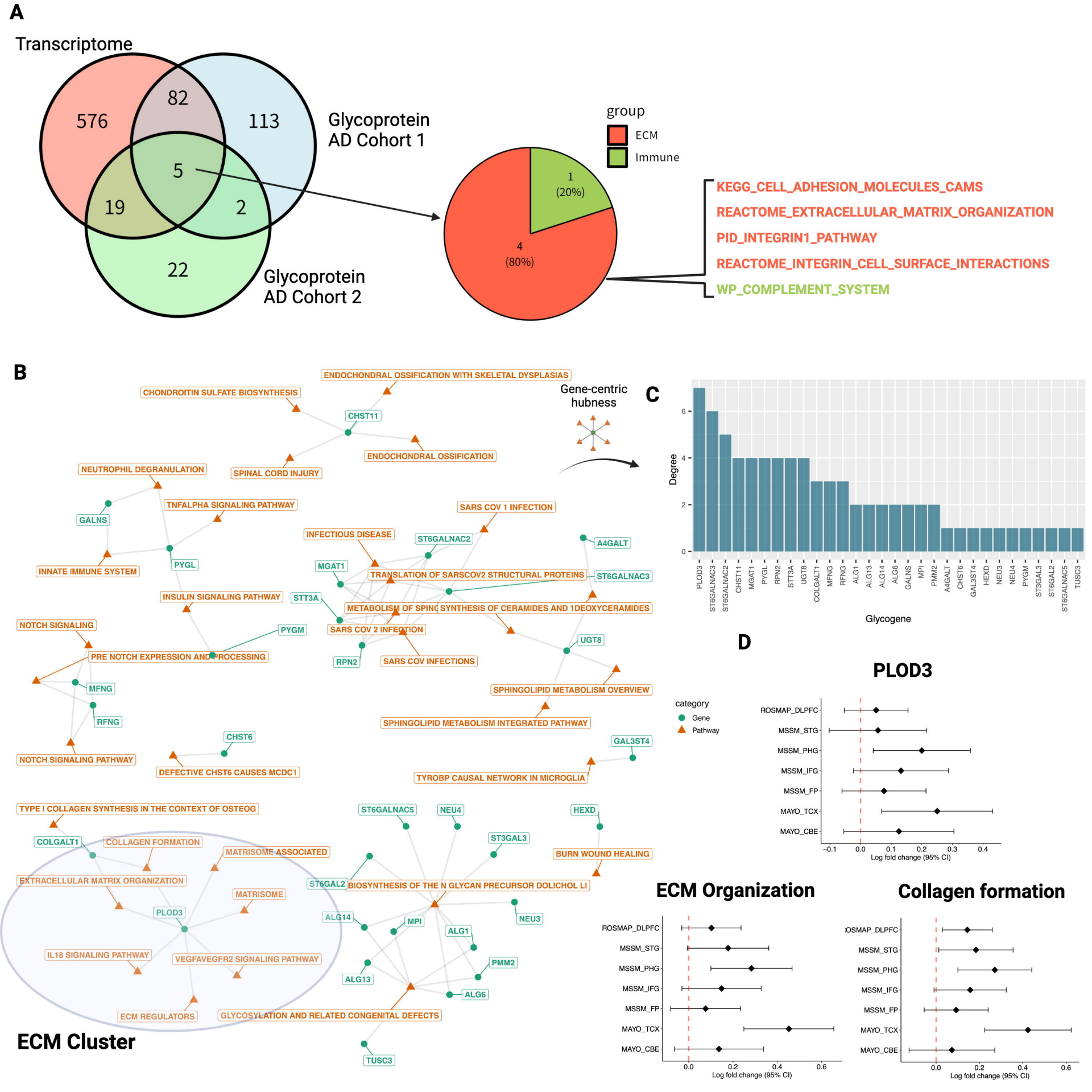
A
Transcriptome
576
82
113
5
19
2
22
Glycoprotein AD Cohort 1
Glycoprotein AD Cohort 2
group
ECM
Immune
1 (20%)
4 (80%)
KEGG_CELL_ADHESION_MOLECULES_CAMS
REACTOME_EXTRACELLULAR_MATRIX_ORGANIZATION
PID_INTEGRIN1_PATHWAY
REACTOME_INTEGRIN_CELL_SURFACE_INTERACTIONS
WP_COMPLEMENT_SYSTEM
B
Gene-centric hubness
ENDOCHONDRAL OSSIFICATION WITH SKELETAL DYSPLASIAS
CHONDROITIN SULFATE BIOSYNTHESIS
CHST11
ENDOCHONDRAL OSSIFICATION
SPINAL CORD INJURY
NEUTROPHIL DEGRANULATION
TNFALPHA SIGNALING PATHWAY
GALNS
INNATE IMMUNE SYSTEM
PYGL
SARS COV 1 INFECTION
INFECTIOUS DISEASE
ST6GALNAC2
A4GALT
MGAT1
TRANSLATION OF SARSCOV2 STRUCTURAL PROTEINS
ST6GALNAC3
INSULIN SIGNALING PATHWAY
STT3A
METABOLISM OF SPING SYNTHESIS OF CERAMIDES AND 1DEOXYCERAMIDES
NOTCH SIGNALING
PYGM
SARS COV 2 INFECTION
UGT8
PRE NOTCH EXPRESSION AND PROCESSING
RPN2
SARS COV INFECTIONS
MFNG
SPHINGOLIPID METABOLISM OVERVIEW
RFNG
SPHINGOLIPID METABOLISM INTEGRATED PATHWAY
CHST6
GAL3ST4
NOTCH SIGNALING PATHWAY
DEFECTIVE CHST6 CAUSES MCDC1
TYROBP CAUSAL NETWORK IN MICROGLIA
TYPE I COLLAGEN SYNTHESIS IN THE CONTEXT OF OSTEOG
ST6GALNAC5
NEU4
HEXD
COLGALT1
COLLAGEN FORMATION
ST3GAL3
MATRISOME ASSOCIATED
BURN WOUND HEALING
EXTRACELLULAR MATRIX ORGANIZATION
ST6GAL2
BIOSYNTHESIS OF THE N GLYCAN PRECURSOR DOLICHOL LI
MATRISOME
PLOD3
ALG14
MPI
NEU3
ALG1
IL18 SIGNALING PATHWAY
VEGFAVEGFR2 SIGNALING PATHWAY
PMM2
ALG13
ALG6
ECM REGULATORS
GLYCOSYLATION AND RELATED CONGENITAL DEFECTS
TUSC3
ECM Cluster
category
Gene
Pathway
C
Degree
Glycogene
PLOD3
ST6GALNAC3
ST6GALNAC2
CHST11
MGAT1
PYGL
RPN2
STT3A
UGT8
COLGALT1
MFNG
RFNG
ALG1
ALG13
ALG14
ALG6
GALNS
MPI
PMM2
A4GALT
CHST6
GAL3ST4
HEXD
NEU3
NEU4
PYGM
ST3GAL3
ST6GAL2
ST6GALNAC5
TUSC3
D
PLOD3
ROSMAP_DLPFC
MSSM_STG
MSSM_PHG
MSSM_IFG
MSSM_FP
MAYO_TCX
MAYO_CBE
Log fold change (95% CI)
ECM Organization
Collagen formation

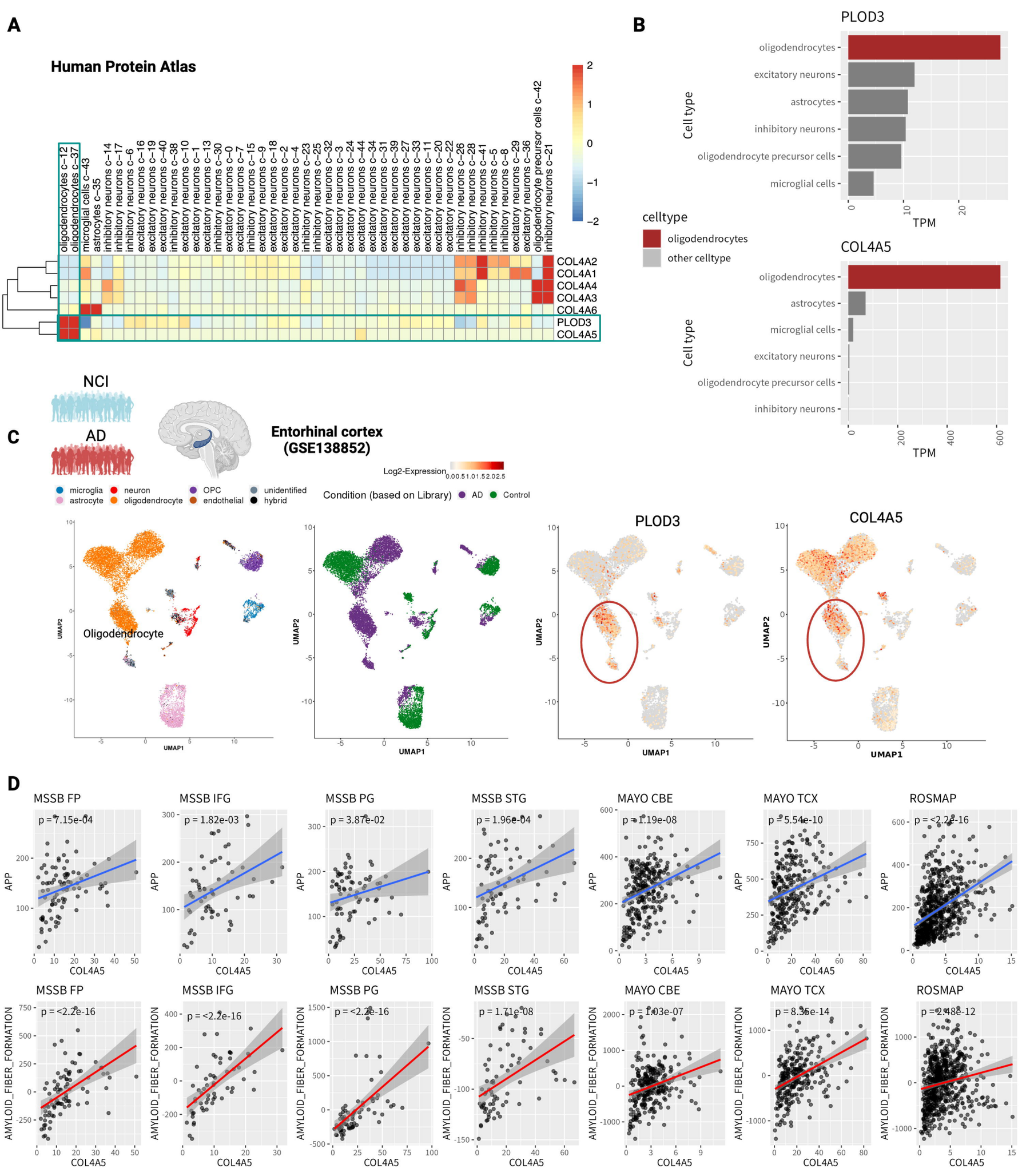
A
Human Protein Atlas
oligodendrocytes c−12
oligodendrocytes c−37
microglial cells c−43
astrocytes c−35
inhibitory neurons c−14
inhibitory neurons c−17
inhibitory neurons c−6
excitatory neurons c−16
excitatory neurons c−19
excitatory neurons c−40
inhibitory neurons c−38
excitatory neurons c−10
excitatory neurons c−1
excitatory neurons c−13
inhibitory neurons c−30
excitatory neurons c−0
excitatory neurons c−7
inhibitory neurons c−15
excitatory neurons c−9
excitatory neurons c−18
excitatory neurons c−2
excitatory neurons c−4
inhibitory neurons c−23
inhibitory neurons c−25
excitatory neurons c−32
excitatory neurons c−3
excitatory neurons c−24
excitatory neurons c−44
excitatory neurons c−34
excitatory neurons c−31
excitatory neurons c−39
excitatory neurons c−27
excitatory neurons c−33
excitatory neurons c−11
excitatory neurons c−20
excitatory neurons c−22
inhibitory neurons c−26
inhibitory neurons c−28
inhibitory neurons c−41
inhibitory neurons c−5
inhibitory neurons c−8
excitatory neurons c−29
excitatory neurons c−36
oligodendrocyte precursor cells c−42
inhibitory neurons c−21
COL4A2
COL4A1
COL4A4
COL4A3
COL4A6
PLOD3
COL4A5
2
1
0
−1
−2
B
PLOD3
Cell type
oligodendrocytes
excitatory neurons
astrocytes
inhibitory neurons
oligodendrocyte precursor cells
microglial cells
0
10
20
TPM
celltype
oligodendrocytes
other celltype
COL4A5
Cell type
oligodendrocytes
astrocytes
microglial cells
excitatory neurons
oligodendrocyte precursor cells
inhibitory neurons
0
200
400
600
TPM
C
NCI
AD
Entorhinal cortex
(GSE138852)
Log2-Expression
0.0 0.5 1.0 1.5 2.0 2.5
microglia
astrocyte
neuron
oligodendrocyte
OPC
endothelial
unidentified
hybrid
Condition (based on Library)
AD
Control
Oligodendrocyte
UMAP1
UMAP2
PLOD3
COL4A5
D
MSSB FP
p = 7.15e-04
MSSB IFG
p = 1.82e-03
MSSB PG
p = 3.87e-02
MSSB STG
p = 1.96e-04
MAYO CBE
p = 1.19e-08
MAYO TCX
p = 5.54e-10
ROSMAP
p = <2.2e-16
APP
COL4A5
MSSB FP
p = <2.2e-16
MSSB IFG
p = <2.2e-16
MSSB PG
p = <2.2e-16
MSSB STG
p = 1.71e-08
MAYO CBE
p = 1.03e-07
MAYO TCX
p = 8.36e-14
ROSMAP
p = 2.48e-12
AMYLOID_FIBER_FORMATION
COL4A5

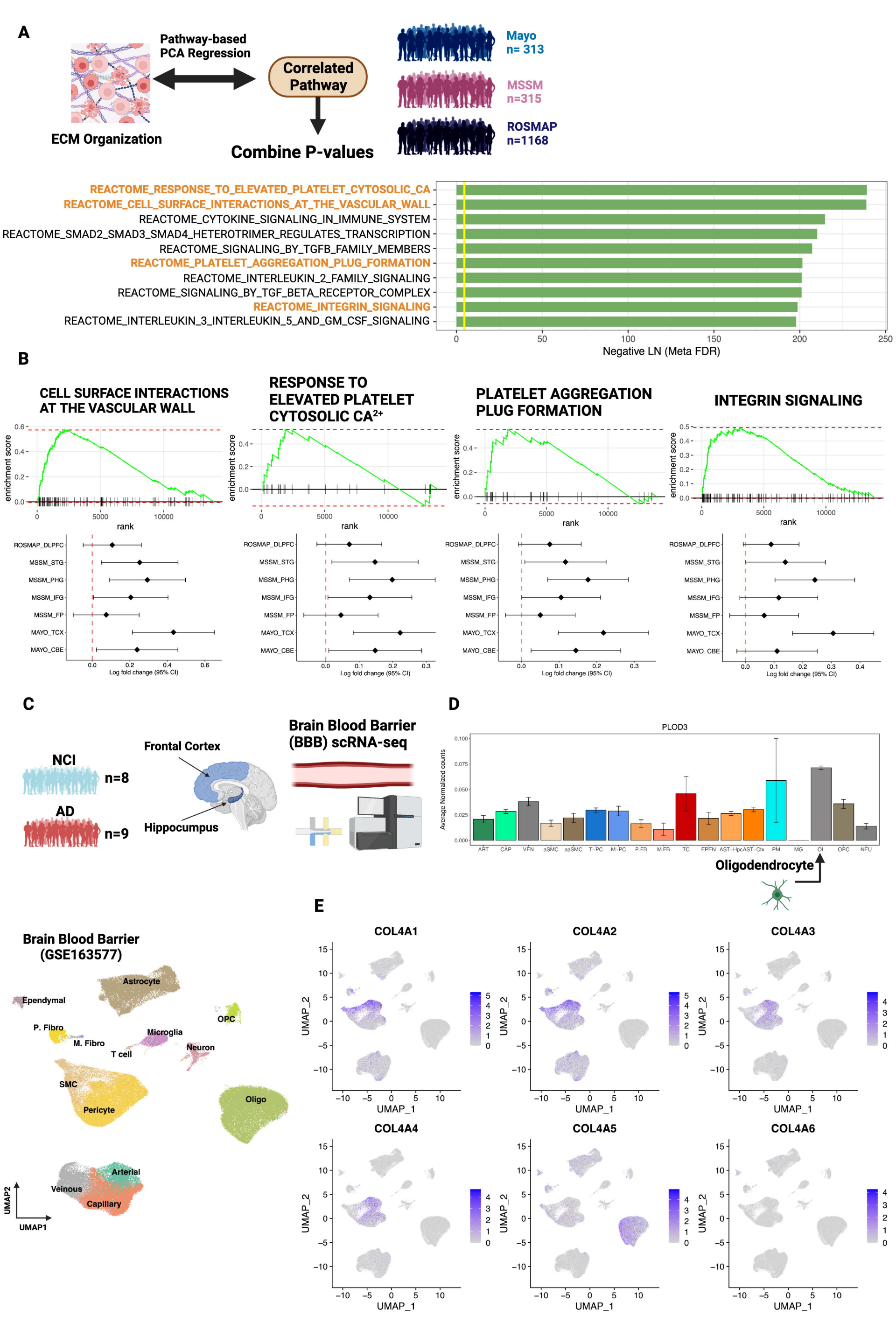
A
Pathway-based PCA Regression
ECM Organization
Correlated Pathway
Combine P-values
Mayo n= 313
MSSM n=315
ROSMAP n=1168
REACTOME_RESPONSE_TO_ELEVATED_PLATELET_CYTOSOLIC_CA
REACTOME_CELL_SURFACE_INTERACTIONS_AT_THE_VASCULAR_WALL
REACTOME_CYTOKINE_SIGNALING_IN_IMMUNE_SYSTEM
REACTOME_SMAD2_SMAD3_SMAD4_HETEROTRIMER_REGULATES_TRANSCRIPTION
REACTOME_SIGNALING_BY_TGFB_FAMILY_MEMBERS
REACTOME_PLATELET_AGGREGATION_PLUG_FORMATION
REACTOME_INTERLEUKIN_2_FAMILY_SIGNALING
REACTOME_SIGNALING_BY_TGF_BETA_RECEPTOR_COMPLEX
REACTOME_INTEGRIN_SIGNALING
REACTOME_INTERLEUKIN_3_INTERLEUKIN_5_AND_GM_CSF_SIGNALING
Negative LN (Meta FDR)
B
CELL SURFACE INTERACTIONS AT THE VASCULAR WALL
RESPONSE TO ELEVATED PLATELET CYTOSOLIC CA2+
PLATELET AGGREGATION PLUG FORMATION
INTEGRIN SIGNALING
enrichment score
rank
ROSMAP_DLPFC
MSSM_STG
MSSM_PHG
MSSM_IFG
MSSM_FP
MAYO_TCX
MAYO_CBE
Log fold change (95% CI)
C
NCI n=8
AD n=9
Frontal Cortex
Hippocampus
Brain Blood Barrier (BBB) scRNA-seq
D
PLOD3
Average Normalized counts
ART CAP VEN aSMC aaSMC T-PC M-PC P.FB M.FB TC EPEN AST-HpcAST-Ctx PM MG OL OPC NEU
Oligodendrocyte
Brain Blood Barrier (GSE163577)
Astrocyte
Ependymal
P. Fibro
M. Fibro
Microglia
T cell
Neuron
OPC
SMC
Pericyte
Oligo
Arterial
Veinous
Capillary
UMAP2
UMAP1
E
COL4A1
COL4A2
COL4A3
COL4A4
COL4A5
COL4A6
UMAP_1
UMAP_2

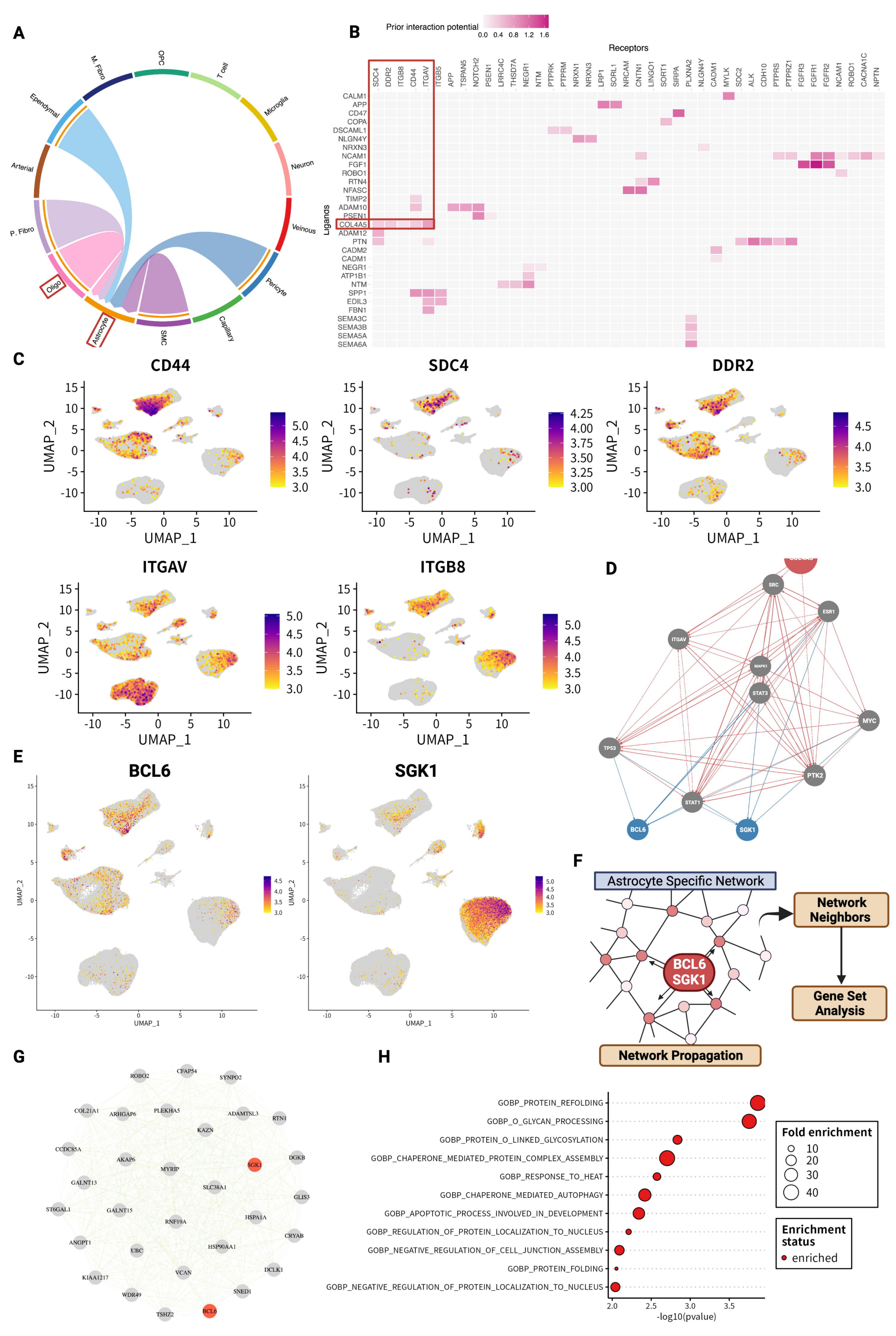
A
M. Fibro
OPC
T cell
Microglia
Neuron
Veinous
Pericyte
Capillary
SMC
Astrocyte
Oligo
P. Fibro
Arterial
Ependymal
B
Prior interaction potential
0.0 0.4 0.8 1.2 1.6
Receptors
Ligands
SDC4 DDR2 ITGB8 CD44 ITGAV ITGB5 APP TSPAN5 NOTCH2 PSEN1 LRRC4C THSD7A NEGR1 NTM PTPRK PTPRM NRXN1 NRXN3 LRP1 SORL1 NRCAM CNTN1 LINGO1 SORT1 SIRPA PLXNA2 NLGN4Y CADM1 MYLK SDC2 ALK CDH10 PTPRS PTPRZ1 FGFR3 FGFR1 FGFR2 NCAM1 ROBO1 CACNA1C NPTN
CALM1 APP CD47 COPA DSCAML1 NLGN4Y NRXN3 NCAM1 FGF1 ROBO1 RTN4 NFASC TIMP2 ADAM10 PSEN1 COL4A5 ADAM12 PTN CADM2 CADM1 NEGR1 ATP1B1 NTM SPP1 EDIL3 FBN1 SEMA3C SEMA3B SEMA5A SEMA6A
C
CD44
SDC4
DDR2
ITGAV
ITGB8
UMAP_1
UMAP_2
D
SRC
ESR1
ITGAV
MAPK1
STAT3
MYC
TP53
PTK2
STAT1
BCL6
SGK1
E
BCL6
SGK1
F
Astrocyte Specific Network
BCL6
SGK1
Network Neighbors
Gene Set Analysis
Network Propagation
G
ROBO2
CFAP54
SYNPO2
COL21A1
ARHGAP6
PLEKHA5
ADAMTSL3
RTN1
KAZN
CCDC85A
AKAP6
MYRIP
SGK1
DGKB
GALNT13
SLC38A1
GLIS3
ST6GAL1
GALNT15
RNF19A
HSPA1A
CRYAB
ANGPT1
UBC
HSP90AA1
DCLK1
KIAA1217
VCAN
SNED1
WDR49
TSHZ2
BCL6
H
GOBP_PROTEIN_REFOLDING
GOBP_O_GLYCAN_PROCESSING
GOBP_PROTEIN_O_LINKED_GLYCOSYLATION
GOBP_CHAPERONE_MEDIATED_PROTEIN_COMPLEX_ASSEMBLY
GOBP_RESPONSE_TO_HEAT
GOBP_CHAPERONE_MEDIATED_AUTOPHAGY
GOBP_APOPTOTIC_PROCESS_INVOLVED_IN_DEVELOPMENT
GOBP_REGULATION_OF_PROTEIN_LOCALIZATION_TO_NUCLEUS
GOBP_NEGATIVE_REGULATION_OF_CELL_JUNCTION_ASSEMBLY
GOBP_PROTEIN_FOLDING
GOBP_NEGATIVE_REGULATION_OF_PROTEIN_LOCALIZATION_TO_NUCLEUS
-log10(pvalue)
Fold enrichment
10
20
30
40
Enrichment status
enriched

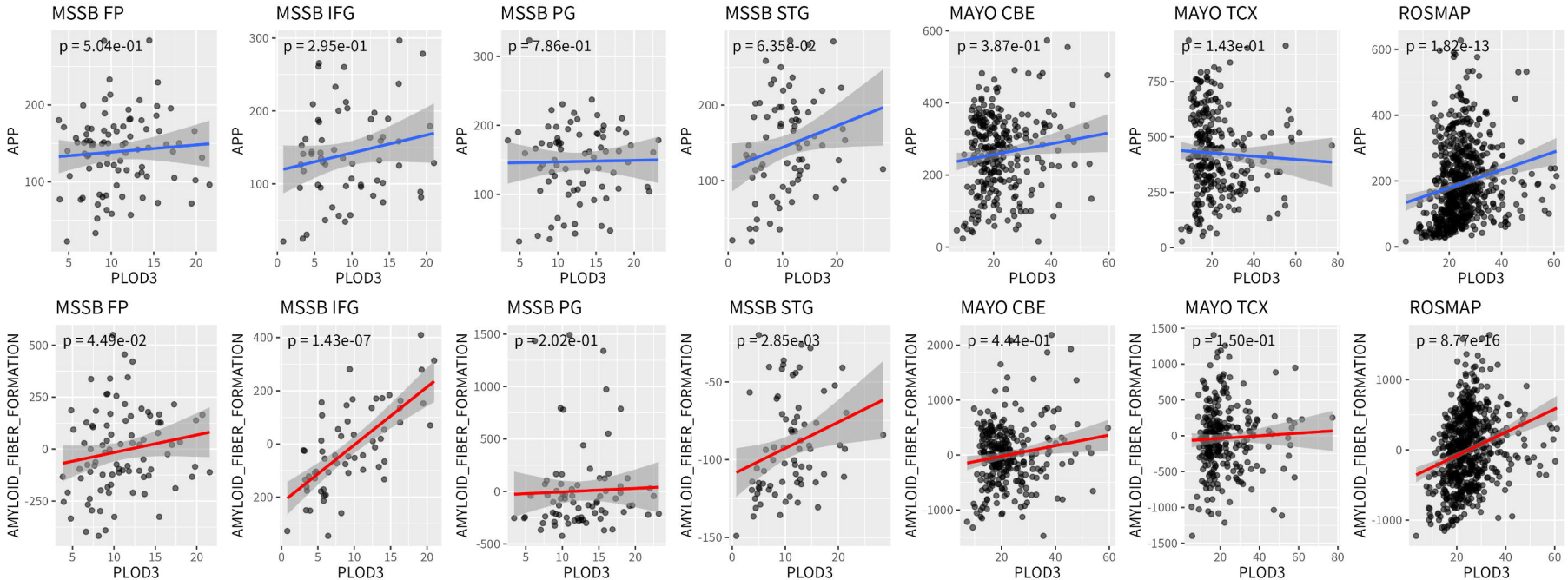
MSSB FP
p = 5.04e-01
MSSB IFG
p = 2.95e-01
MSSB PG
p = 7.86e-01
MSSB STG
p = 6.35e-02
MAYO CBE
p = 3.87e-01
MAYO TCX
p = 1.43e-01
ROSMAP
p = 1.82e-13
APP
PLOD3
MSSB FP
p = 4.49e-02
MSSB IFG
p = 1.43e-07
MSSB PG
p = 2.02e-01
MSSB STG
p = 2.85e-03
MAYO CBE
p = 4.44e-01
MAYO TCX
p = 1.50e-01
ROSMAP
p = 8.77e-16
AMYLOID_FIBER_FORMATION
PLOD3

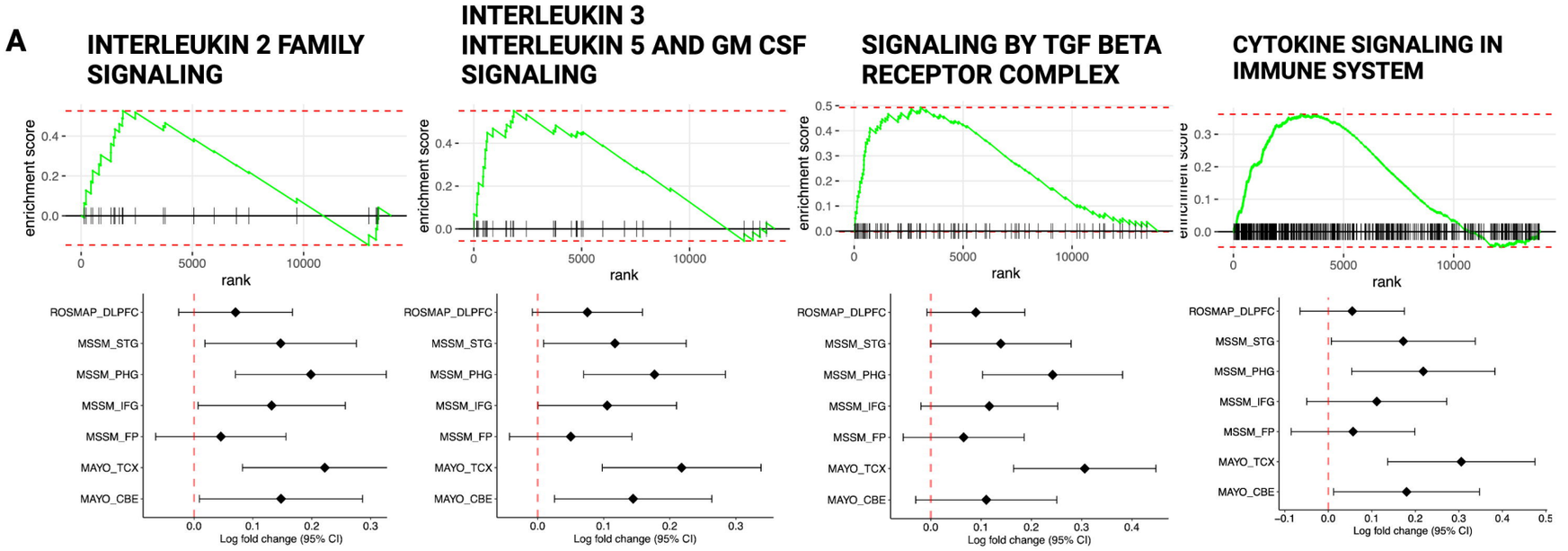
A
INTERLEUKIN 2 FAMILY SIGNALING
INTERLEUKIN 3 INTERLEUKIN 5 AND GM CSF SIGNALING
SIGNALING BY TGF BETA RECEPTOR COMPLEX
CYTOKINE SIGNALING IN IMMUNE SYSTEM
enrichment score
rank
ROSMAP_DLPFC
MSSM_STG
MSSM_PHG
MSSM_IFG
MSSM_FP
MAYO_TCX
MAYO_CBE
Log fold change (95% CI)

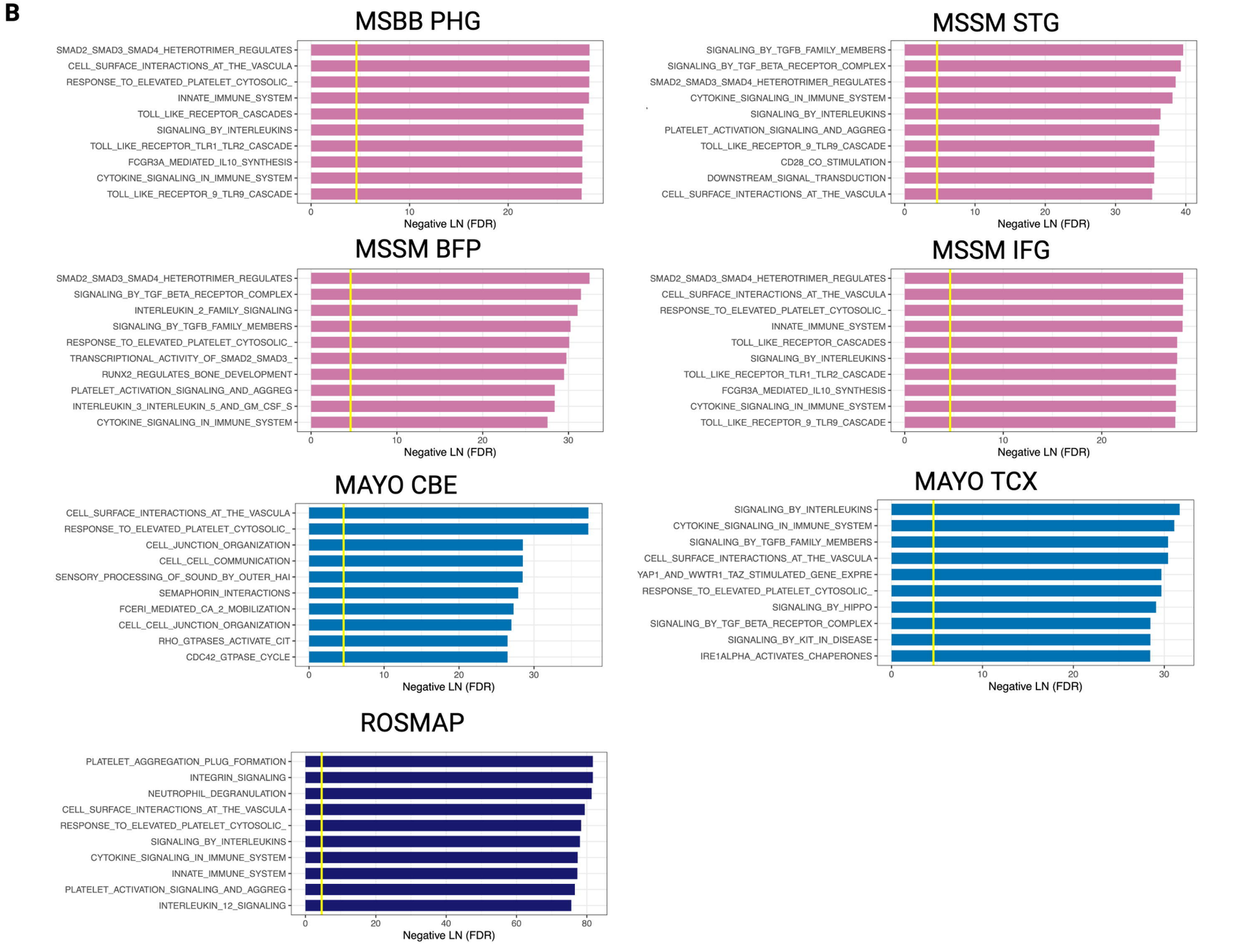
B
MSBB PHG
SMAD2_SMAD3_SMAD4_HETEROTRIMER_REGULATES
CELL_SURFACE_INTERACTIONS_AT_THE_VASCULA
RESPONSE_TO_ELEVATED_PLATELET_CYTOSOLIC_
INNATE_IMMUNE_SYSTEM
TOLL_LIKE_RECEPTOR_CASCADES
SIGNALING_BY_INTERLEUKINS
TOLL_LIKE_RECEPTOR_TLR1_TLR2_CASCADE
FCGR3A_MEDIATED_IL10_SYNTHESIS
CYTOKINE_SIGNALING_IN_IMMUNE_SYSTEM
TOLL_LIKE_RECEPTOR_9_TLR9_CASCADE
MSSM STG
SIGNALING_BY_TGFB_FAMILY_MEMBERS
SIGNALING_BY_TGF_BETA_RECEPTOR_COMPLEX
PLATELET_ACTIVATION_SIGNALING_AND_AGGREG
CD28_CO_STIMULATION
DOWNSTREAM_SIGNAL_TRANSDUCTION
MSSM BFP
INTERLEUKIN_2_FAMILY_SIGNALING
TRANSCRIPTIONAL_ACTIVITY_OF_SMAD2_SMAD3_
RUNX2_REGULATES_BONE_DEVELOPMENT
INTERLEUKIN_3_INTERLEUKIN_5_AND_GM_CSF_S
MSSM IFG
MAYO CBE
CELL_JUNCTION_ORGANIZATION
CELL_CELL_COMMUNICATION
SENSORY_PROCESSING_OF_SOUND_BY_OUTER_HAI
SEMAPHORIN_INTERACTIONS
FCERI_MEDIATED_CA_2_MOBILIZATION
CELL_CELL_JUNCTION_ORGANIZATION
RHO_GTPASES_ACTIVATE_CIT
CDC42_GTPASE_CYCLE
MAYO TCX
YAP1_AND_WWTR1_TAZ_STIMULATED_GENE_EXPRE
SIGNALING_BY_HIPPO
SIGNALING_BY_KIT_IN_DISEASE
IRE1ALPHA_ACTIVATES_CHAPERONES
ROSMAP
PLATELET_AGGREGATION_PLUG_FORMATION
INTEGRIN_SIGNALING
NEUTROPHIL_DEGRANULATION
Negative LN (FDR)

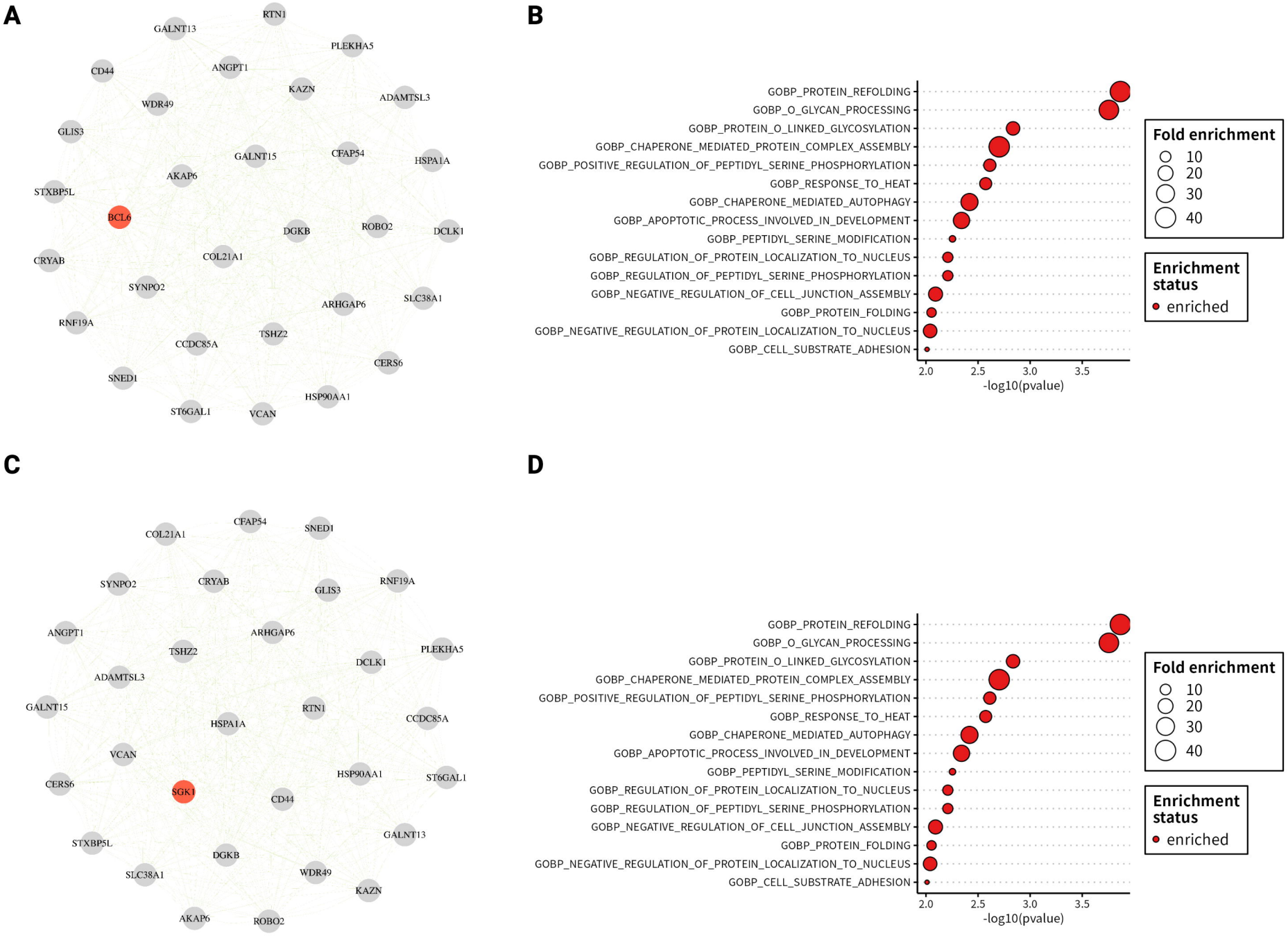
A
RTN1
GALNT13
PLEKHA5
CD44
ANGPT1
KAZN
ADAMTSL3
WDR49
GLIS3
GALNT15
CFAP54
HSPA1A
AKAP6
STXBP5L
BCL6
DGKB
ROBO2
DCLK1
CRYAB
COL21A1
SYNPO2
ARHGAP6
SLC38A1
RNF19A
TSHZ2
CCDC85A
CERS6
SNED1
HSP90AA1
ST6GAL1
VCAN
B
GOBP_PROTEIN_REFOLDING
GOBP_O_GLYCAN_PROCESSING
GOBP_PROTEIN_O_LINKED_GLYCOSYLATION
GOBP_CHAPERONE_MEDIATED_PROTEIN_COMPLEX_ASSEMBLY
GOBP_POSITIVE_REGULATION_OF_PEPTIDYL_SERINE_PHOSPHORYLATION
GOBP_RESPONSE_TO_HEAT
GOBP_CHAPERONE_MEDIATED_AUTOPHAGY
GOBP_APOPTOTIC_PROCESS_INVOLVED_IN_DEVELOPMENT
GOBP_PEPTIDYL_SERINE_MODIFICATION
GOBP_REGULATION_OF_PROTEIN_LOCALIZATION_TO_NUCLEUS
GOBP_REGULATION_OF_PEPTIDYL_SERINE_PHOSPHORYLATION
GOBP_NEGATIVE_REGULATION_OF_CELL_JUNCTION_ASSEMBLY
GOBP_PROTEIN_FOLDING
GOBP_NEGATIVE_REGULATION_OF_PROTEIN_LOCALIZATION_TO_NUCLEUS
GOBP_CELL_SUBSTRATE_ADHESION
2.0
2.5
3.0
3.5
-log10(pvalue)
Fold enrichment
10
20
30
40
Enrichment status
enriched
C
CFAP54
SNED1
COL21A1
SYNPO2
CRYAB
GLIS3
RNF19A
ANGPT1
ARHGAP6
TSHZ2
PLEKHA5
DCLK1
ADAMTSL3
GALNT15
RTN1
CCDC85A
HSPA1A
VCAN
HSP90AA1
ST6GAL1
CERS6
SGK1
CD44
GALNT13
STXBP5L
DGKB
SLC38A1
WDR49
KAZN
AKAP6
ROBO2
D
GOBP_PROTEIN_REFOLDING
GOBP_O_GLYCAN_PROCESSING
GOBP_PROTEIN_O_LINKED_GLYCOSYLATION
GOBP_CHAPERONE_MEDIATED_PROTEIN_COMPLEX_ASSEMBLY
GOBP_POSITIVE_REGULATION_OF_PEPTIDYL_SERINE_PHOSPHORYLATION
GOBP_RESPONSE_TO_HEAT
GOBP_CHAPERONE_MEDIATED_AUTOPHAGY
GOBP_APOPTOTIC_PROCESS_INVOLVED_IN_DEVELOPMENT
GOBP_PEPTIDYL_SERINE_MODIFICATION
GOBP_REGULATION_OF_PROTEIN_LOCALIZATION_TO_NUCLEUS
GOBP_REGULATION_OF_PEPTIDYL_SERINE_PHOSPHORYLATION
GOBP_NEGATIVE_REGULATION_OF_CELL_JUNCTION_ASSEMBLY
GOBP_PROTEIN_FOLDING
GOBP_NEGATIVE_REGULATION_OF_PROTEIN_LOCALIZATION_TO_NUCLEUS
GOBP_CELL_SUBSTRATE_ADHESION
2.0
2.5
3.0
3.5
-log10(pvalue)
Fold enrichment
10
20
30
40
Enrichment status
enriched